UNIVERSIDADE D
COIMBRA

Sofia Correia Silva Santos

# DIMENSIONAMENTO E ESTUDO DE UM SIMULADOR SOLAR PARA TREINO DE ACLIMATAÇÃO DE ATLETAS

**Dissertação no âmbito do Mestrado Integrado em Engenharia Mecânica na Especialidade de Energia e Ambiente, orientada pelo Professor Doutor Adélio Manuel Rodrigues Gaspar e pelo Professor Doutor Gonçalo Jorge Vieira Nunes Brites, apresentada ao Departamento de Engenharia Mecânica da Faculdade de Ciências e Tecnologia da Universidade de Coimbra**

Fevereiro de 2023

1 2 9 0

FACULDADE DE CIÊNCIAS E TECNOLOGIA
UNIVERSIDADE D COIMBRA

# Design and study of a solar simulator for athletes' acclimation training

Submitted in Partial Fulfilment of the Requirements for the Degree of Master in Mechanical Engineering in the speciality of Energy and Environment

# Dimensionamento e estudo de um simulador solar para treino de aclimatação de atletas


**Author**

**Sofia Correia Silva Santos**

**Advisors**

**Professor Doutor Adélio Manuel Rodrigues Gaspar**

**Professor Doutor Gonçalo Jorge Vieira Nunes Brites**


**Jury**

| | |
|---|---|
| **President** | **Professor Doutor Amândio Manuel Cupido Santos**<br>**Professor [Auxiliar] da Universidade de Coimbra** |
| **Vowels** | **Professor Doutor Gonçalo Jorge Vieira Nunes Brites**<br>**Professor da Universidade de Coimbra**<br>**Professor Doutor Avelino Virgílio Fernandes Monteiro de Oliveira**<br>**Professor Coordenador do Instituto Politécnico de Coimbra** |

**Coimbra, February, 2023**

“Give me six hours to chop down a tree and I will spend the first four sharpening the axe”

Abraham Lincon

# ACKNOWLEDGEMENTS

O trabalho que aqui se apresenta só foi possível graças à colaboração e apoio de algumas pessoas, às quais não posso deixar de prestar o meu reconhecimento.

Em primeiro lugar, quero agradecer aos meus pais e avós pelo apoio incondicional e a todos os níveis, sem o qual o meu percurso académico não seria possível.

Quero também agradecer aos meus amigos, do Secundário, de Erasmus e de Coimbra, que marcaram e continuam a marcar a minha vida.

Por fim, gostaria de agradecer aos meus orientadores pela sua enorme disponiblidade e apoio durante a realização desta dissertação.

# Abstract

Several studies have shown that performing acclimation training allows athletes to improve their physical performance during sports competitions carried out under adverse environmental conditions. The majority of acclimation training take into account the high levels of air temperature and air humidity.

It is common practice in acclimation training to replicate ambient conditions with high air temperature and relative humidity. Nonetheless, high solar irradiance is often neglected. This fact was brought to the attention of a racewalking athlete after training in the climate chamber of the *Industrial Aerodynamics Laboratory* (LAI) belonging to the *Association for the Development of Industrial Aerodynamics* (ADAI). As a result, the need to increase the climate chamber's range of simulation capacities emerged.

For that purpose, a study on already existing technology and a design study for a solar simulator to be implemented in the climate chamber were carried out. The design study involved: measuring the radiation emitted by a luminaire from an existing solar simulator in photometric and radiometric units; modeling the luminaire through the mathematical manipulation of the measured data; validating the model; importing the model to *DIALux*; and studying the optimal configuration of the solar simulator through.

Hence, with the study of existing technology, it was concluded that each luminaire should consist of a metal halide lamp, a parabolic reflector, and a Fresnel lens.

In the design study, through a direct comparison between the measured data and the equivalent values obtained by the simulation, the model was successfully validated. Even though it was found to be undersized. It was concluded that in order to reach irradiance values above 800W/m$^2$ in the majority of the athlete's back area, twenty-one luminaires would be necessary (with lamps powered by 575W), placed 1.25m distant from the athlete. To reach irradiance values just above 600W/m$^2$, only twelve luminaires would be needed under the same conditions. The luminaires were assigned an inclination angle of 60° with the vertical, in order to represent an adequate direction of natural solar radiation in a competitive scenario.

**Keywords:** Solar Simulator, Acclimation Training, Climate Chamber, DIALux, Radiometry.

# Resumo

Vários estudos têm demonstrado que a realização de treino de aclimatação permite aos atletas melhorar o seu rendimento físico durante competições desportivas realizadas com condições ambientais adversas. A maioria dos treinos de aclimatação tem em conta os efeitos nocivos de altos níveis de temperatura e humidade do ar. No entanto, despreza os efeitos nocivos relacionados com os ganhos térmicos por radiação solar. Este facto foi mencionado por uma atleta de marcha, após treinar na câmara climática do *Laboratório de Aerodinâmica Industrial* (LAI), pertencente à *Associação para o Desenvolvimento de Aerodinâmica Industrial* (ADAI). Assim, surge a necessidade de aumentar o leque de capacidades da câmara climática referida.

Neste sentido, foi feito um estudo de tecnologia existente e um estudo de dimensionamento de um simulador solar a ser implementado na câmara climática. O estudo de dimensionamento envolveu: a medição da radiação emitida por uma luminária, de um simulador solar já existente, em unidades fotométricas e radiométricas; o cálculo de um coeficiente de conversão de unidades fotométricas para unidades radiométricas; a modelação da luminária em estudo, através da manipulação matemática dos valores medidos; a validação do modelo; a importação do modelo para o *DIALux*; e o estudo da configuração óptima. Com o estudo de tecnologia existente, conclui-se que cada luminária deveria ser constituída por uma lâmpadas de iodetos metálicos, um refletor parabólico e uma lente Fresnel. No estudo de dimensionamento, através de uma comparação direta entre os valores medidos e os valores calculados pela simulação, o modelo construído foi validado com sucesso, apesar de se encontrar subdimensionado.

Através do estudo de configuração, chegou-se à conclusão que, para atingir valores de irradiação superiores a 800W/m$^2$ na grande maioria da área das costas do atleta, seriam necessárias vinte e uma luminárias (com lâmpadas com 575W de potência elétrica), colocadas a uma distância de 1.25 metros do atleta. Para atingir valores de irradiação superiores a 600 W/m$^2$, seriam apenas precisas doze luminárias, nas mesmas condições. Às luminárias foi atribuída uma inclinação de 60º com a vertical, com o intuito de replicar uma direção representativa da radiação solar em situação de competição.

**Palavras-chave:** Simulador Solar, Treino de Aclimatação, Câmara Climática, DIALux, Radiometria.

# Contents

# LIST OF FIGURES

# LIST OF TABLES

# LIST OF SIMBOLS AND ACRONYMS

## List of Symbols

d – Distance from the light source [m]

$E_e$ – Irradiance [$W/m^2$]

$E_v$ – Illuminance [lx]

$I_v$ – Luminous intensity [cd]

R – Correlation coefficent [-]

$u_0$ – Uniformity index [-]

X – Horizontal coordinate [m]

Z – Vertical coordinate [m]

## List of Acronyms

ADAI – Association for the Development of Industrial Aerodynamics

AM – Air Mass

CTCV – Tecnologial Center of Ceramics and Glass

HMI – Hydrargyrum Medium-arc Iodide lamp

IR – Infrared Radiation

LAI – Industrial Aerodynamics Laboratory

LED – Light Emitting Diode

NR – Not Reported

UV – Ultraviolet Radiation

VIS –Visible Radiation

# 1. INTRODUCTION

## 1.1. Historical context

One of the oldest fields of study is the human body's response to its surrounding climate conditions (Y. Xiao et al., 2022). By studying previous responses, it is possible to predict future behavior.

With the initial purpose of continuing the studies on the human body's response to different climate conditions to improve indoor thermal comfort, in 1994, the *Association for the Development of Industrial Aerodynamics* (ADAI[1]) installed a climate chamber on its *Industrial Aerodynamics Laboratory* (LAI[2]). LAI's climate chamber can recreate different indoor and outdoor climate conditions. Since its inauguration, the climate chamber has been in continuous development, often undergoing improvements to its facilities, according to the needs of the activities that are being carried out.

More recently, the climate chamber has started to be used in acclimation training for high competition athletes. Acclimation training is an important part of the global training of an athlete that is going to compete in a climate with extreme conditions. This specific training, which aims the increase of body thermoregulation efficiency, consists of provoking a physiologic adaptation in the athletes' body to reduce the physiologic strain, which it is caused by different climate conditions imposed by the climate chamber. Thus, making the athletes more adapted to the environmental conditions they face when competing, they may improve their performance and consequently they can reach better results (Dionísio, 2021).

LAI's climate chamber was already used to assist athletes of various modalities, preparing them for competitions such as 2016 Olympic Games in Rio de Janeiro, 2019 World Athletics Championship in Doha and 2020 Olympic Games in Tokyo (Pires António, 2020).

## 1.2. Motivation and Objectives

Until this year, the climate chamber allowed the control of the ambient temperature, the relative humidity and the supply airflow. During last year's trainings, one of the race walking athletes reported that these features alone are insufficient to replicate all the

[1]ADAI – *Associação para o Desenvolvimento de Aerodinâmica Industrial*.
[2] LAI – *Laboratório de Aerodinâmica Industrial*.

environmental conditions they face during their sports competitions, making the use of LAI's climate chamber inadequate for a proper acclimation training of that modality.

Athletes of outdoor sports, like racewalking and others, can be subjected to prolonged sun exposure during a sports event. The effects of direct solar radiation have significant importance in the thermal balance of an individual and in their internal body behaviors, consequently, also have a significant effect on the athlete's performance. Yet, these effects have been not fully adressed until now. In this context, emerges the necessity of enhancing the quality of the athletes' acclimation training, by adding a new feature to the climate chamber simulation system, enlarging its simulation capacities.

Training in a climate chamber that can replicate the environmental conditions that the athletes will face during the competitions can help them adjust their internal body behaviors while also training themselves to compete in extreme climatic conditions.

The purpose of this dissertation is to study and to design of a radiant system that replicates solar radiation, i.e., a solar simulator, that if installed in LAI's climate chamber would expand its range of simulated climate conditions. Since this system is to be used to study the response of athletes to solar radiation and to improve the quality of their acclimation training, the author first intends to study the influence of solar radiation on athletes' performance and acclimation training. Thereafter, the writing of an overview of solar simulation and solar simulators (their typical composition, principal types of light sources used over the years and previous solar simulators) will be considered.

To study the optimal design of a solar simulator to be installed in the climate chamber, the aim is to utilize the software *DIALux*, which is a lighting design software that provides its light calculation results in photometric units. To allow the radiometric units to be taken into account, the author also intends to obtain a conversion between irradiance (in $W/m^2$) and illuminance (in lux), based on measurements of the emitted radiation of an existing solar simulator's luminaire. Since the radiation spectrum also influences the athletes' performance, a comparison between the spectrums of the measured luminaire and the sun's radiation will be held.

# 2. LITERATURE REVIEW

This chapter presents the theoretical concepts of how athletes are affected by radiation and what they can to prevent and diminish the deleterious effects caused by an exposure to adverse weather conditions.

## 2.1. Influence of solar radiation on athletes' performances and heat acclimation

Due to natural evolution, the human being is able to accustom themself to the environment. The human body's physiological and biochemical processes are influenced by signals received from the surroundings and by the physical interactions with them.

Since the surrounding conditions suffer fluctuations, so does the human body's internal behavior and, consequently, the athletes' performances. In order to prepare them so they can achieve their peak performance during sports events, the impact of the surroundings' conditions must be studied.

Nonetheless, there are still other variables, not related to the environmental conditions, that influence performance, such as motivation, exhaustion, air quality, etc.

### 2.1.1. Thermal balance: influence of direct solar radiation

Environmental solar radiation is a fundamental condition to be considered in the fluctuation of the athletes' performances, and it depends on the climate conditions, the geographic location and the time of the day.

When exposed to the sun, an individual receives thermal energy from solar radiation, mainly from direct solar radiation (that is the share of solar radiation that reaches the surface without being diffused), this addition of energy has an impact on the individual's thermal balance. The human thermal balance is commonly described by Equation 2.1 (adapted from (Yasmeen & Liu, 2019)), in which all variables are expressed in W/m$^2$ (m$^2$ refers to the superficial skin area).

$$M - W = L + (K + C + R) + E \pm S \quad (2.1)$$

Where: $M$ is the metabolic rate; $W$ is the work exerted on the environment; $L$ is the heat exchange in the respiratory tract; $K$, $C$ and $R$ represent the heat exchange by conduction, convection and radiation, respectively ($R$ can be divided in short wave radiation, received

from direct solar radiation, and long wave radiation, emitted by the body itself and received from the atmosphere and the surrounding surfaces); E is the heat exchange through the evaporation of water/sweat through the skin; and $S$ symbolizes the heat storage in the body. When S equals zero, the individual experiences thermal balance, otherwise the individual might suffer from thermal stress.

As homeothermic animals, humans are able to maintain their core temperature constant to a normal function value. When in a harsh environment, it reacts physiologically towards this goal, that is, if the human body is under heat stress its physical response promotes heat loss, if it is under cold stress its physical response promotes conservation/production of internal heat. The four main behaviors aimed at controlling the internal temperature in a dynamic environment are vasodilation and sweating, as a response to heat stress, and vasoconstriction and shivering, as a result of cold stress.

In sporting events, athletes commonly suffer heat stress due to their high metabolic rate. In outdoor events, the effects of heat stress can be even more worrisome since the adverse environmental conditions, such as prolonged exposure to direct solar radiation, high solar radiation intensity, high air temperatures or high relative humidity levels, cannot be neither controlled nor manipulated. Intensive exercise under heat can lead to an unnaturally high body temperature, in other words, hyperthermia. Heat illnesses, due to hyperthermia, can appear at various levels of severity, from heat cramps and fatigue to heat exhaustion, or even heat stroke. These heat stress related ailments negatively affect the athlete's performance.

The literature suggests that certain athlete performance aspects, particularly endurance exercise capacity, decrease with the level of and exposure time to solar radiation to which they are subjected while exercising. This impairment of performance can be due to the increase in skin temperature that occurs when the athlete is exposed to direct solar radiation. Even though an elevated skin temperature is an effect of vasodilatation, a too high increase in skin temperature causes a decrease of the skin - body core temperature gradient. As consequence, a greater skin blood flow is required, which entails a higher cardiovascular strain, which in its turn leads to poorer aerobic exercise performance (Otani et al., 2016).

The increase in skin temperature is not only owed to direct solar radiation, but also to low wind speed and high relative humidity and ambient air temperature, which can occur

during competitions. In light of this observation, Otani et al. (2016), state that it is reasonable that the impact of solar radiation on endurance exercise performance depends on air temperature, with a decrease in endurance capacity at high but not at low air temperatures. Moreover, the same author points out that although the unfavorable effects of prolonged solar radiation exposure appear to be more significant at high direct solar radiation intensities, even low levels of direct solar radiation reveal to have a negative impact on endurance performance, in hot environments.

### 2.1.2. Circadian rhythms: influence of visible radiation

All living beings have biological clocks that allow them to predict the oscillations of the environment so that their physiology can respond in a preventive and anticipatory way, with the adaptative advantage that this entails (Lucas-Sánchez et al., 2012).

Biological clocks are regulated by external factors called "zeitgebers" (which is the German term for "time markers") and they generate the endogenous rhythms of the individual's body. Physical activity, time of nutrition and social and psychological factors are some zeitgebers of the human biological clock, but the main zeitgeber is the environmental natural light-dark cycle. Consequently, the majority of human internal rhythms are synchronized with solar time. For this reason, they are known as "circadian rhythms" or "circadian cycles", which is a term from the Latin language that means behavioral, mental and physical changes in the human body that follow a time cycle of approximately twenty-four hours.

Circadian rhythms are presented in several physiological processes such as body temperature fluctuation, hormone secretion, sleep-wake cycle and activity patterns (Vitosevic, 2017). These processes have a great influence on athlete's response; therefore, one can conclude that athletic performance depends on the time of day when the exercise is performed.

Body temperature is regarded as the leading indicator of physical performance, due to their direct relation. According to Teo et al. (2011), the increase of the core temperature increases energy metabolism, improves muscle compliance and facilitates actin-myosin

cross bridging[3]; Vitosevic (2017) adds that its increase is also in line with the increase in coordination, reaction time, muscle strength, cardiovascular efficiency, anaerobic power and flexibility of joints. These internal changes influence positively individuals' physical performance. Thus, the daily peak performance occurs around the same time as the daily peak of body temperature; literature shows that these peaks tend to happen in the early evening.

It is important to highlight that the increase in body temperature which is beneficial to physical performance is due to internal body changes, that is, is the natural increase of the daily oscillation cycle. A too high increase in body temperature caused by adverse environmental conditions can lead to hyperthermia, which reduces performance, as mentioned in subchapter 2.1.1.

Another factor of athletic performance is the hormone levels. There are three hormones of great importance, namely testosterone, cortisol and melatonin. Melatonin is the hormone that induces sleep, and is responsible for controlling the sleep-wake cycle.

Out of time exposure to light can disrupt the melatonin production cycle, and consequently can result in the desynchronization of the internal circadian cycles. When athletes travel to compete in a distant location, they get exposed to a different light-dark schedule, while their biological clock stays synchronized with the previous location's light cycle. That is to say, the athletes' circadian rhythms and the current light-dark cycle became out of sync, which leads to a decline in their physical performance. To ensure they achieve their best performance during sports competitions, athletes need to nullify the symptoms caused by jet lag (for instance, fatigue, irritability, loss of focus, sleep loss, etc.), by adjusting their biological clock to the current time zone (Yamanaka et al. (2006) ).

The resynchronization period varies with the individual but always takes several days. High performance athletes generally have heavy schedules, thus it is of utmost importance to make the phase of resynchronization as brief as possible. To work towards this goal, it is recommended to establish the normal daily behavior exposure to sunlight rhythms activities in relation to the local time, of the place where the sports competition will take place, since the endogenous mechanisms are manipulable. It is then crucial to

[3] The actin-myosin cross bridge referes to the sequence of events in the thick and thin filaments of a muscle that results in its contraction.

understand the factors that influence them and how they exert that influence (Vitosevic, 2017).

Training in a climate chamber with, among other systems, a solar simulator can help the athletes to adjust their endogenous rhythms, without the need to travel through several time zones, while also training themselves to compete under extreme climate conditions.

### 2.1.3. Heat acclimation

Physiological heat strain can result from: physical interactions with the surroundings' harsh environmental conditions, such as high air temperature, high air humidity, exposure to intense solar radiation; high physical work rate, which implies high metabolic heat production; or/and heavy clothing, which can inhibit the body's ability to thermoregulate (Schleh et al., 2018).

Athletes that compete in hot environments often suffer from heat stress. Over time, as they continue to exercise under heat stress, their physiological heat strain increases. This elicits an impairment in their physical performance, since in order to prevent hyperthermia, their ability to maintain work output degenerates (Ko et al., 2020).

To inhibit a significant reduction in performance, and avoid heat related illnesses, the effects of heat stress must be lessened. To do so, the athletes' ability to acclimate must be enhanced, in other words, their heat dissipation capacity and readiness to perform in hot environments must be improved (Ko et al., 2020).

Two similar strategies to mitigate the effects of heat stress are Heat Acclimation and Heat Acclimatization. Both consist of recurrent elevations of core and skin temperatures caused by repeated and systematic ambient heat exposures, exercise sessions or a combination of both, in order to subject the athletes to stressful conditions that evoke physiological adaptations, improving their thermoregulatory and cardiovascular systems (Ööpik et al., 2014; Périard et al., 2016). What differentiates the two methods is where the training takes place. In Heat Acclimation training, the heat environmental adaptation is achieved in a climate chamber that simulates a hyperthermal environment, while in Heat Acclimatization the training occurs in a natural environment.

Acclimatization training does not allow the control of the conditions of the athletes' training, so, athletes must travel to the location of the sporting event several weeks prior, to

acclimatize themselves. Acclimation training is advantageous when athletes have tight schedules that restrain them from traveling in advance or having their training dependent on weather conditions.

#### 2.1.3.1. Heat acclimation training strategies and time course of adaptation

In traditional heat acclimation training, the thermal load applied is constant during the whole process, leading to physiologic habituation. This causes the acclimation training to progressively lose effectiveness as adaptations occur. A more recent approach consists of increasing the thermal loads in accordance with the evolution of the adaptations, to maintain body temperature at a fixed value throughout acclimation training, regardless of the athlete's acclimation state. This approach, known as controlled hyperthermia or isothermic heat acclimation, has shown to induce more rapid and complete heat adaptation than traditional methods (Périard et al., 2015).

The heat acclimation process can be divided into three periods: short-term (<7days), medium-term (8 to 14 days) and long-term (>15days) acclimation (Périard et al., 2015). In traditional heat acclimation training protocols, most of the adaptations (approximately 80%) occur in the first week of heat acclimation and are optimized in the following periods, due to the gradual reduction of physiological strain (Klous et al., 2020). Since short-term acclimation results in similar, but with a shorter extent, adaptations than a full acclimation process, high performance athletes often opt for short-term acclimation (R. R. Pryor et al., 2021).

Professional athletes also prefer to acclimate themselves preceding the competition, as adaptations induced by heat acclimation training are temporary, and fade quickly and progressively if the acclimation training is not continued (J. L. Pryor et al., 2019). The adaptations that decay most swiftly are also the ones that develop most rapidly during acclimation training (Périard et al., 2016).

#### 2.1.3.2. Physiological adaptations

The extent of the physiological adaptations resulting from heat acclimation differs depending on the individual's factors (such as their initial acclimation state, fitness level, age and sex) and training conditions (namely, exercise intensity, duration and frequency, and number of heat exposures) (Périard et al., 2016 and Relf et al., 2020).

The main physiological adaptations that occur during exercise-heat acclimation training are an increase of plasma volume, a lowering of exercising heart rate, a decrease of core and skin temperature, an increase of sweating rate and a more evenly distributed along the body, a betterment of thermal comfort and, as result, an improvement in exercise capacity. The time course of these adaptations can be seen in Figure 2.1.

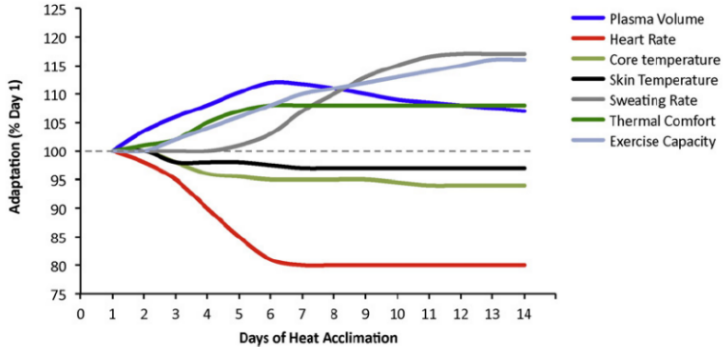


**Figure 2.1** Time course of physiological adaptations of a traditional exercise-heat acclimation (Périard et al., 2016).

In addition to the adaptations mentioned in the Figure 2.1 , it is also worth the shift of the onset of sweating, which occurs at a lower core temperature, that is, it occurs earlier and, as a result, so does the skin's evaporative cooling (Périard et al., 2016). Another adaptation that also entails lower body temperature and diminished cardiovascular strain is the plasma volume increase. An increase of the plasma volume improves the heat transfer from core to skin, which reduces the undesirable rise in core temperature. In addition, according to Périard et al., (2016), plasma volume expansion also contributes to the decrease of the heart rate which implies the increase of the aerobic capacity.

Heat acclimation also improves the relationship of thirst to body water needs, thus improving individuals' ability to remain hydrated when suffering thermal stress (Zhang & Zhu, 2021). Dehydration magnifies the adverse physiological effect caused by heat stress, because dehydration jeopardizes skin blood flow, and therefore it impairs the body's ability to dissipate heat.

## 2.2. Experimental modeling of Solar Radiation

### 2.2.1. Solar Radiation

Solar radiation, as the name suggests, is the radiation that comes from the sun. The sun emits radiation in the form of electromagnetic waves, with different wavelengths. Like any

other body, it emits radiation due to its temperature that, in the surface, is approximately, 5800 K. The sun spectrum, out of the atmosphere, resembles the spectrum of a black body at the same temperature. The spectrum is the range of all types of electromagnetic radiation that are distinguished by their wavelength range (G2V Optics, 2022).

Due to the Earth's atmosphere, the surface of the Earth does not receive all the radiation emitted by the sun, being partially absorbed and scattered by the atmosphere molecules, and thereby the spectrum is modified.

The solar spectrum on the surface of the Earth is not constant, depending on the length of the radiation path through the atmosphere, and this length varies with the sun beams' incident angle. The solar spectrum on Earth is also affected by the composition of the atmosphere, which can be affected by weather conditions. Therefore, separate times and locations imply different solar spectrums.

The main share of the spectrum that reaches Earth's surface is called Optical Radiation. This band is divided into three ranges of radiation: Ultraviolet Radiation (UV), in radiation waves with a length from 100nm to 400nm; Visible Radiation or light (VIS), in wavelengths from 400nm to 700nm[4]; and Infrared Radiation (IR), in wavelengths from 700nm to 1mm. Most of the optical radiation is concentrated in the Visible and Infrared ranges, and it has its peak in the Visible part of the spectrum (G2V Optics, 2022.). Figure 2.2 illustrates the modifications that the solar spectrum suffers due to the filtering of atmospheric gases, as well as the comparison between the solar spectrum, out of the atmosphere, and the radiation spectrum of a black body at the same temperature.

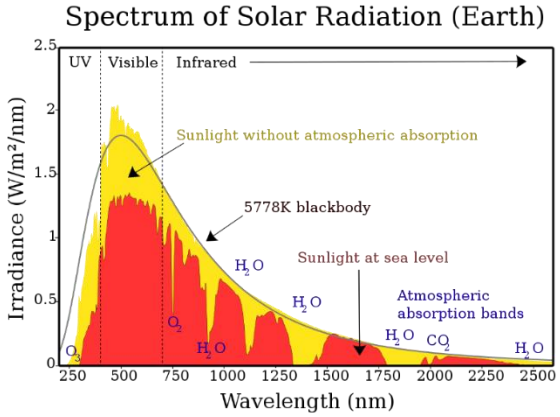


**Figure 2.2** Solar Radiation Spectrum (G2V Optics, 2022.).

[4] The wavelength value that defines the end of the visible range and the beginning of the infrared range differs according to the author. However, the accepted values are always comprehended between 700 nm and 800nm.

## 2.2.2. Solar Simulators

A Solar Simulator is a radiative system designed to replicate the natural sunlight in its spectrum and intensity, which is placed in an indoor test facility, under controlled laboratory conditions. Solar simulators emerge as the need of studying the effects of solar radiation on photosensitive materials' processes. Due to the natural variations of the climatic conditions, the natural sunbeam on the Earth's surface is not constant, which inhibits the use of an outdoor test facility for reliable studies when those require steady-state and controlled conditions. Nowadays, this technology has a great importance in several fields of study, including industrial material analysis, photovoltaic devices testing, medical and biological research.

### 2.2.2.1. Composition of Solar Simulators

A solar simulator is commonly constituted by the following major components: power supply, light source and control system. In some cases, they may also contain optical filters, reflectors and lenses, if necessary, to meet the radiation output requirements. (Wang, 2014b). So, the configuration varies from solar simulator to solar simulator.

An electrical power supply is an electrical device used to supply electrical loads. This device's main function is to convert the electrical current from a source to the accurate voltage, frequency and current to the supply load (Wat Electrical, 2018). In solar simulators the electrical load is the light source and control devices, thereby the power supply is associated with it.

The light source is the most crucial element of the solar simulator, in virtue of being the component that emits radiation, and it may consist of a single or multiamp system. Historically, many types of lamps, with different working principles, have been used as light sources. Each type has its own advantages and drawbacks, so there is no best light source to be used in solar simulators in general. The selection of the light source must consider the type and application of the solar simulator, as well as factors like the light source spectrum quality, life cycle, cost, efficiency, heat production and ease of use (Tawfik et al., 2018).

Solar simulators require control devices to be operated. The configuration and complexity of the control system depend on the light source in use. Certain lamps are made with a technology that allows them to be able to vary their radiation power, others always emit with a fixed value of intensity.

Every unique type of artificial light source has its characteristic electromagnetic spectrum, and even though some resemble the solar spectrum on Earth, none of them can perfectly replicate it. The modification of the lamps' spectrum, to reach the solar simulator's desired outcome spectrum, can be done using optical filters. An optical filter is a device that rejects the unwanted radiation, by absorbing or reflecting it, while transmitting the remainder.

A lamp reflector is a structure that surrounds and is fixed to the light source. When applied to solar simulators, its function is to redirect the lamps' scattered radiation beams, thus being partially responsible for the solar simulator output radiation direction, uniformity, and intensity. They are frequently made of or coated by a highly reflective metal, like aluminum, to assure that the maximum amount of radiation is redirected instead of absorbed by the material. Two of the most commonly used reflectors in solar simulators are the ellipsoidal reflector (for concentrated light beams) and parabolic reflector (for collimated light beams).

Another device meant to guide the radiation beams is the lens. A lens is an optical device, typically made of glass, which redirects the radiation beams that pass through it by refraction. In solar simulators, Fresnel lenses are used as concentrators or as collimators, i.e., they can concentrate parallel beams into a single point, or they can align in parallel beams emitted from a focal point.

### 2.2.3. Light Sources of Solar Simulators

The light source of a solar simulator may consist of a single or multiple lamp system, multiple lamp systems can be mono or multiple light source systems. In multisource systems, more than one type of lamp is used with the purpose of improving accuracy. Historically, several types of radiation emitting devices have been employed in solar simulators, namely carbon arc lamp, high pressure sodium vapor lamp, argon arc lamp, quartz tungsten halogen lamp, mercury xenon lamp, xenon arc lamp, metal halide lamp, light emitting diode (LED) and supercontinuum laser (Deepak et al., 2020).

According to Deepak et al. (2020), the most frequent types of light sources used in solar simulators for terrestrial thermal applications are xenon arc lamps, quartz tungsten halogen lamps and metal halide lamps and LEDs.

## Xenon arc lamp

A xenon arc lamp is a gas discharge lamp. This type of lamp emits radiation by passing electricity through the ionized and highly compressed xenon gas that is contained in the lamp envelope (the lamp envelope also contains small amount of mercury particles). The lamp envelope is made of quartz, which is a glass material able to withstand high pressures and high temperatures. A scheme of the lamp configuration can be seen in the Figure 2.3 (a). Xenon arc lamps produce an extremely bright white light, with a spectrum that closely matches the solar spectrum in the UV and Visible ranges. Solar simulators that have xenon arc lamps at their light sources often need optical filters to attenuate the pics of radiation in the IR range, which can be seen in the Figure 2.3 (b), and cooling systems due to the high temperatures that this type of lamps produce. Moreover, the energy consumption of these lamps is high, and their operation demands a stable power supply.

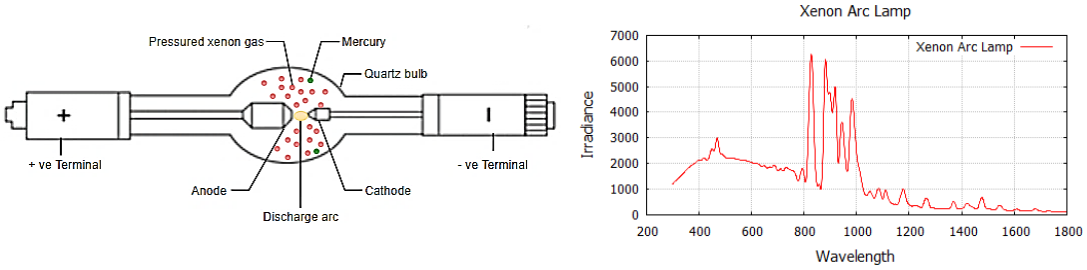


**Figure 2.3 a)** Design of a xenon arc lamp, adapted from (Sobek & Werle, 2019) **b)** Xenon arc lamp typical emission spectrum (TS-Space Systems, n.d.).

Xenon arc lamps started to be used in solar simulators in 1961 (Esen et al., 2017). Due to the excellent characteristics of its output radiation, this lamp is still currently used in solar simulators when these require high intensity and spectrum match quality, and when the high cost of operation is not an issue.

## Quartz tungsten halogen lamp

A quartz tungsten halogen lamp is a type of incandescent lamp. It produces radiation through the heat up of its tungsten filament, caused by the passage of electric current. When a certain temperature is achieved, some particles of the filament material evaporate and then react with the halogen gas to produce light. A considerable amount of the evaporated tungsten returns to the filament after reacting, and it is then recycled. This cycle prolongs the lamp lifetime, when compared with traditional incandescent lamps. The Figure 2.4 (a) shows the configuration of these types of lamps. These lamps have their peak of emissions in the IR range of the spectrum and barely emit in the UV range. Their color temperature is

much inferior than the sun's, therefore, although their spectrum resembles the sunlight, it has significant differences, as it can be seen in the Figure 2.4 (b).

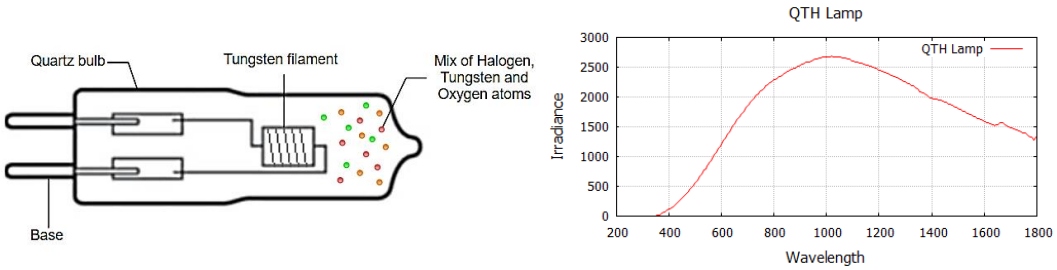


**Figure 2.4 a)** Design of a quartz tungsten halogen lamp, adapted from (Sobek & Werle, 2019) **b)** Quartz tungsten halogen lamp typical emission spectrum (TS-Space Systems, n.d.).

The radiation emission of these lamps is a steady process thanks to the simplicity of the lamps' working principle. The intensity is easily controlled via simple adjustments in the power supply. These lamps began to be implemented in solar simulator devices in 1962 (Esen et al., 2017), and nowadays they are commonly used in multi-source solar simulators or in solar simulators with lower spectrum requirements.

**Metal halide lamp**

The metal halide lamp, like the xenon arc lamp, is a gas discharge lamp. The principal difference is the composition of the filled gas. A metal halide lamp contains a mix of metal halide vapors and mercury in tiny amounts in its inner tube. The configuration of a typical metal halide lamp can be seen in the Figure 2.5 (a). The use of a certain number of different metals particles results in an electromagnetic spectrum remarkably similar to the solar spectrum in the UV and VIS regions, however, it has several peaks all over the three ranges. Some models come with a UV-block glass filtering, to face the lamp's strong emissions on the shortwave range of the spectrum. Solar simulators with metal halide lamps can also be equipped with IR-stop filters, to correct the high peak of emitted radiation in that zone, which is visible in the Figure 2.5 (b).

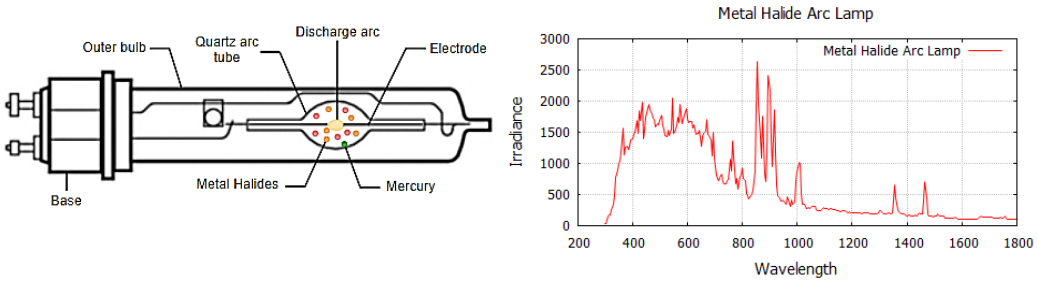


**Figure 2.5 a)** Design of a metal halide lamp, adapted from (Sobek & Werle, 2019) **b)** Metal halide lamp typical emission spectrum (TS-Space Systems, n.d.).

Metal halide lamps have lower spectral quality than the xenon arc lamp, but lower costs. They also have higher spectral quality and higher costs than tungsten halogen lamps. They started to be implemented in solar simulators in 2005 (Esen et al., 2017), and continue to be used in modern solar simulators.

**Light emitting diode**

A light emitting diode (LED) is a solid-state semiconductor device whose working principle is electroluminescence. It emits light when an electric current passes through it, the higher the current flow, the higher its emitted intensity. LEDs devices began to be applied in solar simulators in 2003 (Esen et al., 2017), after the appearance of the high-power LEDs. The configuration of a typical LED of this type can be seen in the Figure 2.6.

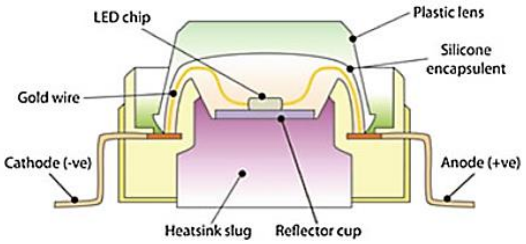


**Figure 2.6** Design of a typical high-power LED (Dutta Gupta & Agarwal, 2017).

The emitted spectrum of these devices differs from the spectrums of the traditional lamps. LEDs emit radiation in a short bandwidth of wavelengths; thus, they are often called monochromatic. Because there is a large variety of LEDs that emit at different wavelengths, it is possible to combine a diverse set of LEDs to reproduce any required discrete[5] spectrum, by embedding specific LEDs (Dutta Gupta & Agarwal, 2017). These devices can emit in the UV, in the VIS or in the IR range, depending on their type. The type of single light emitting diode that most copies the natural sun light is the White LED, albeit the quantities of emitted radiation out of the visible range is quite negligible. Solar simulators with LED as their light source have a dynamic and relatively simple control system, that can vary not only the outcome intensity but also the outcome spectrum almost instantaneously. Nonetheless, for high intensity solar simulation applications, fully LED systems are not the preferred light source yet, as high radiation intensity values are difficult to achieve by relying only on LED devices (Bodnár et al., n.d.). The intensity increases with the increase of the current that

[5] A discrete spectrum, in contrast to a continuous spectrum, contains gaps between wavelengths.

flows through the semiconductor, but an excess of energy flow also makes the LED overheat and overheating significantly reduces the device's lifetime.

The LED is the most recent of the four presented light emitting technologies, it is in constant development and is expected to have immense importance in the future of solar simulators. The tendency is for the LEDs to replace the traditional light sources over time.

**Comparison of the most commonly used light sources**

Table 2.1 and Table 2.2 show a comparison between distinguishing aspects of the most used light sources, and a brief summary of advantages and drawbacks, respectively.

**Table 2.1.** Comparison of the most commonly used light sources' distinguishing aspects.

| | **Working principle** | **Wavelength range (nm)** | **Color Temperature (K)[6]** | **Average lifetime (hours)** | **Additional requirements[7]** | **Average conversion efficiency[8] (%)** | **Average light efficiency (%)[9]** |
|---|---|---|---|---|---|---|---|
| **Xenon arc lamp** | Electrical discharge through an ionized pressured gas | 185 - 2600 | 6000 | 400 - 3500 | Ballast and igniter | 19 | 4.4 – 13.5 |
| **Quartz tungsten halogen lamp** | Incandescence | 250 - 2500 | 2100 - 3350 | 35 – 480 | - | 10 | 3.5 |
| **Metal halide lamp** | Electrical discharge through an ionized pressured gas | 200 - 2600 | 4000 - 6000 | 1000 - 6100 | Ballast and igniter | 25 | 9.5 - 17 |
| **LED** | Electroluminescence | Wildly variable | Wildly variable | 50000 – 100000 | Led driver | 40 - 50 | 11 – 43.9 |
| **Reference (s)** | (Tawfik et al., 2018) [14.b2] | (Deepak et al., 2020) | (Tawfik et al., 2018) | (Wang, 2014) (Tawfik et al., 2018) | (Tawfik et al., 2018) | (Tawfik et al., 2018) [DiaLux_site] | (Wikipedia, n.d.) |

[6] A lamp's color temperature corresponds to a black body radiator temperature with a maximum irradiance which is obtained at the same wavelength as the light source (Tawfik et al., 2018).

[7] Xenon arc lamps and Metal halide lamps may only require an igniter if the ballast is electromagnetic. The use of an electronic ballast prevents the need of an ignitor.
Quartz tungsten halogen lamps require dimmers if their radiative intensity needs to be variable.

[8] The conversion efficiency expresses the ratio between the radiative power emitted by the light source, which reaches the target area, and the electrical power consumed by it.

[9] The light efficiency is the ratio between the luminous power, which is the share of the radiative power emitted solely by the visible range wavelengths, and electrical power that supplies the light source.

**Table 2.2.** List of advantages and drawbacks of the most commonly used light sources.

| | Advantages | Drawbacks | Reference(s) |
|---|---|---|---|
| **Xenon arc lamp** | 1. Stable spectra.<br>2. Excellent spectra match in UV and VIS.<br>3. Power variation has a low effect on spectral balance.<br>4. Produces a collimated high-intensity light beam. | 1. More complex and expensive power supply, when compared with the other light sources.<br>2. Peak of radiation in the IR range that may need to be filtered.<br>3. Unstable lamp output due to power supply instabilities.<br>4. Aging affects the output spectrum.<br>5. Risk of explosion due to the high-pressured gas.<br>6. Relatively expensive. | (Wang, 2014)<br>(G2V Optics, 2022) |
| **Quartz tungsten halogen lamp** | 1. Good spectra match in IR.<br>2. Simple power supply.<br>3. Relatively inexpensive. | 1. Poor spectra match in UV and VIS.<br>2. Higher Overheating risk.<br>3. Short lifetime<br>4. Ceasing production in European countries and others, | (Wang, 2014)<br>(G2V Optics, 2022) |
| **Metal halide lamp** | 1. Good spectral quality that closely matches the sun spectrum.<br>2. High temporal stability.<br>3. Long lifetime.<br>4. Lower gas pressure than xenon arc lamps. | 1. Peak of radiation in the UV range that may need to be filtered.<br>2. More complex power supply than quartz tungsten halogen lamps and LEDs.<br>3. Low collimation quality.<br>4. Relatively expensive. | (Wang, 2014)<br>(G2V Optics, 2022) |
| **LED** | 1. Versatile control of the flux emission and radiation spectrum.<br>2. Stable output.<br>3. Simple power supply.<br>4. Less power consumption and operating cost, due to higher efficiency.<br>5. Small size and directional light emission.<br>6. Outstanding longer lifetime than any other light sources. | 1. Discrete spectrum.<br>2. Lower radiation light intensity.<br>3. Output energy, efficiency and lifetime drop sensitively with the operation temperature rising of the junction. | (Wang, 2014)<br>(Dutta Gupta & Agarwal, 2017)<br>(G2V Optics, 2022) |

Both gas discharge lamps are able to reach out to sun's colour temperature, whereas quartz tungsten halogen lamps cannot attain so high values. The color temperature of metal halide lamps depends on their inner tube mix of metal gases composition; therefore, it slightly changes with the lamp's model. In LED sets, this aspect depends on their type, since the emitted wavelength range also relies on it. Consequently, their color temperature can be wildly variable. LEDs have by far the longest lifetime and highest efficiency values, followed by the metal halide lamps; quart tungsten halogen lamps have the shortest and the lowest. However, halogen lights compensate for it with their low price, and lack of complex

additional requirements. These lamps are known as the cheapest light source, while the xenon arc lamps are usually the costliest ones.

Among traditional lamps used in solar simulators light sources, the xenon arc lamps are the ones with the best spectral quality, metal halide lamps have the second best spectrum match with the solar spectrum, and the quartz tungsten halogen lamps the worst. With the recent LED technology, it is achievable to have solar simulators with not only excellent spectral quality but also with controllable and adjustable output spectrum. From the reading of the Table 2.2, it is possible to see that "in the design of modern solar simulators which have low spectrum and intensity requirements, quartz tungsten halogen lamp and metal halide arc lamp are superior to xenon lamp", as it was stated by Wang (2014). Although it has a higher spectral quality, higher efficiency and longer lifetime, a system formed by metal halide lamps and their additional requirements may not always be preferred over one with quartz tungsten halogen lamps as it light source. For applications that do not require too high intensity levels of radiation, but excellent spectral quality, LEDs seem to be an adequate light source solution. These devices can also be seen in multi-light source systems, such as quartz tungsten halogen lamps – LEDs combine system. The implementation of LED devices corrects the deficiency of the halogen lamps' spectral match in the ultraviolet and visible part of the spectrum; the use of halogen lamps allows the solar simulator to achieve high values of light intensity, which the LEDs alone cannot.

### 2.2.4. Previous Solar Simulators

Over the years, different types and models of solar simulators have been designed and developed for different applications, such as testing and development of solar cells, research on photosynthetic organisms, material testing, etc. (Grandi et al., 2014). More recently, they began being used to study the effects of solar radiation on thermal comfort and physical performance, and in acclimation training of high performance athletes.

**Solar Simulators designed for traditional applications**

Table 2.3, Table 2.4, Table 2.5, Table 2.6 and Table 2.7 depict a summary of some previous solar simulators found in literature, that use as their light source Xenon arc lamps, Halogen lamps, Metal halide lamps, LED and a combination of Halogen lamps and LED, respectively. The solar simulators presented in the tables were designed for the traditional applications of solar simulators.

**Table 2.3.** Summary of previous solar simulators using Xenon arc lamps as their light source.

| | Year | Type of reflector(s) | Type of lens(es) | Number of lamps | Power consumed per lamp [kW] | Peak flux [kW/m$^2$] | Maximum average flux [kW/m$^2$] | Conversion efficiency [%] | Distance from light source to the testing surface [m] | Testing surface area [m$^2$] | Reference(s) |
|---|---|---|---|---|---|---|---|---|---|---|---|
| **Xenon arc lamp** | 2017 | Parabolic | Fresnel | 12 | 7 | $6.36 \cdot 10^3$ | NR[10] | 27.6 | NR | 0.031 | (W. Wang et al., 2017) |
| | | | | | | $7.22 \cdot 10^3$ | NR | 26.7 | NR | 0.062 | |
| | 2018 | Ellipsoidal | - | 7 | 2.5 | 194 | NR | NR | 2 | 0.058 | (Martíne, 2018) |
| | 2018 | Non-coaxial ellipsoidal | - | 7 | 6 | $2.51 \cdot 10^3$ | NR | 27.9 | 0.744 | 0.002 | (J. Xiao et al., 2018) |
| | 2019 | Ellipsoidal | - | 7 | 10 | $9.2 \cdot 10^3$ | $5.1 \cdot 10^3$ | 20.6 | 0.85 | 0.003 | (Jin et al., 2019) |
| | | | Fresnel | | | 0.94 | 0.94 | NR | NR | 12 | |
| | 2019 | Ellipsoidal | - | 12 | 7 | $9.26 \cdot 10^3$ | $3.74 \cdot 10^3$ | 32.5 | 0.735 | 0.003 | (Dai et al., 2019) |
| | 2020 | Ellipsoidal | - | 13 | 10 | $11.27 \cdot 10^6$ | $1.05 \cdot 10^6$ | 31.6 | 1.5852 | 0.031 | (Zhu et al., 2020) |
| | 2020 | Ellipsoidal | - | 7 | 4 | $7.74 \cdot 10^3$ | $2.93 \cdot 10^3$ | 29.6 | 0.2124 | 0.003 | (Li et al., 2020) |
| | 2021 | Non-coaxial ellipsoidal | - | 3 | 10 | $8.57 \cdot 10^3$ | $1.21 \cdot 10^3$ | 31.8 | 0.744 | 0.008 | (J. Wang et al., 2021) |

[10] NR – Not Reported

**Table 2.4.** Summary of previous solar simulators using Halogen lamps as their light source.

| | Year | Type of reflector(s) | Type of lens(es) | Number of lamps | Power consumed per lamp [kW] | Peak flux [kW/m$^2$] | Maximum average flux [kW/m$^2$] | Conversion efficiency [%] | Distance from light source to the testing surface [m] | Testing surface area [m$^2$] | Reference(s) |
|---|---|---|---|---|---|---|---|---|---|---|---|
| **Halogen lamp** | 1974 | Ellipsoidal | Fresnel | 143 | 0.3 | 1.02 | 1.02 | 3.5 | 4.6 | 1.44 | (NASA, 1974) |
| | 2012 | Parabolic | - | 9 | 0.05 | NR | 1.004 | NR | 0.42 | 0.0156 | (Namin et al., 2012) |
| | 2013 | Cylindrical | - | 30 | 0.4 | NR | NR | NR | 0.23 | 1.73 | (Mahmoud Shatat, 2013) |
| | 2014 | Parabolic | - | 36 | 0.05 | 1 | 1 | NR | 0.14 | NR | (Salam et al., 2014) |
| | 2015 | Cylindrical | - | 20 | 0.5 | 1.016 | 1.016 | NR | 0.673 | NR | (Irwan et al., 2015) |
| | | | | | | 0.413 | 0.413 | NR | 1.194 | | |
| | 2016 | NR | - | 20 | 0.3 | NR | 0.645 | NR | 1 | 0.92 | (Velmuruga n & Kalaivanan, 2016) |
| | 2018 | Parabolic | - | 16 | 0.05 | NR | 1 | NR | 0.32 | 0.133 | (Yandri, 2018) |

**Table 2.5.** Summary of previous solar simulators using Metal halide lamps as their light source.

| | Year | Type of reflector(s) | Type of lens(es) | Number of lamps | Power consumed per lamp [kW] | Peak flux [kW/m$^2$] | Maximum average flux [kW/m$^2$] | Conversion efficiency [%] | Distance from light source to the testing surface [m] | Testing surface area [m$^2$] | Reference(s) |
|---|---|---|---|---|---|---|---|---|---|---|---|
| **Metal halide lamp** | 2009 | Cylindrical | - | 15 | 1.2 | 1 | NR | NR | NR | 3.75 | (Mei et al., 2009) |
| | 2010 | Ellipsoidal | - | 7 | 1.5 | 60 | 45 | NR | NR | 0.113 | (Codd et al., 2010) |
| | 2011 | Parabolic | - | 188 | 0.4 | NR | 1 | NR | 2 | 3 | (Meng et al., 2011) |
| | | | | | | NR | 1 | NR | 1.75 | 4.6 | |
| | 2014 | Ellipsoidal | - | 7 | 6 | 927 | 499 | 28.6 | NR | 0.024 | (Gallo et al., 2017) |
| | 2015 | Ellipsoidal | - | 1 | 6 | 700 | 100 | 20 | NR | 0.003 | (Gallo et al., 2017) |
| | | | | 7 | | $2.8 \cdot 10^3$ | $1.6 \cdot 10^3$ | 50 | NR | | |
| | 2016 | NR | - | 6 M.H. lamps of 1 kW & 6 M.H. lamps of 2 kW | | 0.924 | 0.79 | NR | 1 | 7.56 | (Sabahi et al., 2016) |
| | 2021 | Parabolic | - | 20 | 0.36 | 1.031 | 1.017 | NR | NR | 0.32 | (Colarossi et al., 2021) |
| | | | | | | 1.038 | 0.995 | | | 1.36 | |
| | | | | | | 1.038 | 0.993 | | | 1.8 | |

**Table 2.6.** Summary of previous solar simulators using Light emitting diodes as their light source.

| | Year | Type of reflector(s) | Type of lens(es) | Number of light emitting diodes | Power consumed per LED [kW] | Peak flux [kW/m$^2$] | Maximum average flux [kW/m$^2$] | Conversion efficiency [%] | Distance from light source to the testing surface [m] | Testing surface area [m$^2$] | Reference(s) |
|---|---|---|---|---|---|---|---|---|---|---|---|
| **LED** | 2009 | - | NR | NR | NR | 0.59 | NR | NR | 0.65 | 0.048 | (Bliss et al., 2009) |
| | 2012 | - | NR | 1024 | NR | NR | 1.015 | NR | 0.003 | 0.0156 | (Namin et al., 2012) |
| | 2012 | - | NR | 1024 | NR | NR | 1.01 | NR | 0.003 | 0.0156 | |
| | 2012 | - | NR | 1024 | NR | NR | 0.41 | NR | 0.003 | 0.0156 | |
| | 2012 | - | NR | 1024 | NR | NR | 0.415 | NR | 0.003 | 0.0156 | |
| | 2012 | - | NR | 1024 | NR | NR | 0.81 | NR | 0.003 | 0.0156 | |
| | 2020 | - | NR | 19 | NR | NR | NR | NR | NR | 0.003 | (Samir et al., 2020) |
| | 2022 | - | Hyper-hemispherical aplanatic & plane-convex | 19 | NR | Around 1.036 | NR | NR | 0.1 | 0.001 | (Sun et al., 2022) |

**Table 2.7.** Summary of previous solar simulators using Halogen lamps and Light emitting diodes as their light source.

| | Year | Type of reflector(s) [11] | Type of lens(es) | Number of lamps & light emitting diodes | Power consumed per LED [kW] | Peak flux [kW/m$^2$] | Maximum average flux [kW/m$^2$] | Conversion efficiency [%] | Distance from light source to the testing surface [m] | Testing surface area [m$^2$] | Reference(s) |
|---|---|---|---|---|---|---|---|---|---|---|---|
| **LED & Halogen lamp** | 2009 | NR | - | NR | NR | 1.5 | NR | NR | 0.65 | 0.048 | (Bliss et al., 2009) |
| | 2012 | NR | - | 18 H. lamps of 0.05 kW & 1024 LEDs | | NR | 1.04 | NR | 0.065 | 0.0156 | (Namin et al., 2012) |
| | 2014 | NR | NR | 8 H. lamps of 0.05kW & 75 LEDs | | NR | NR | NR | NR | 0.03 | (Kim et al., 2014) |
| | 2014 | "cheap rectangular aluminum light guide" | NR | 1 H. lamps of 0.075 kW & 20 LEDs | | 1.5 | NR | NR | 0.065 | 0.0156 | (Grandi et al., 2014b) |
| | | | | | | 1.15 | | | 0.135 | | |
| | | | | | | 0.873 | | | 0.2 | | |
| | 2020 | NR | NR | 8 H. lamps of 0.05 kW & 36 High Power LEDs of 0.003kW | | 1.06 | 0.951 | NR | 0.08 from the LED matrix | 0.023 | (Namin et al., 2012) |

[11] Even though it is not specified in the articles, it is very common for small halogen lamps to be incorporated into parabolic reflectors.

Hodder & Parsons, (2006) studied the effects of solar radiation on thermal comfort by using four metal halide lamps of 1kW each to replicate solar conditions, reporting that 1kW/m$^2$ of irradiance has been reached. Otani et al. used a system of sixty seven metal halide lamps of 0.36kW each to conduct two studies (in 2019 and in 2021), both focused on the influence of solar radiation on the exercise capacity in hot environments. The maximum irradiance value described in these articles is 0.8kW/m$^2$ (Otani et al., 2020, 2021). Also, to study the impact of heat on human physical work capacity, in 2022, Foster et al. used three metal halide lamps of 1kW each, obtaining an average radiation of 0.807kW/m$^2$ across the exposed individual's body regions (Foster et al., 2022).

The three solar simulators described are ceiling mounted, and their more specific characteristics (such as type of reflectors used, peak flux, conversion efficiency, etc.) are not mentioned in the corresponding articles, since they focus on the individual's response.

**Solar Simulators designed for athletes' acclimation training**

Besides the solar simulators of these articles, there are also companies that have solar simulator systems designed for athletes' acclimation training available for purchase. The following information was gathered by consulting the manufacturers' websites and catalogs or by direct contact.

*Hönle* proposes two similar solutions. Their main characteristics are presented in Table 2.8. *Hönle* solutions, for a solar simulator designed for acclimation training of athletes, only differ in the wattage of the lamp model in use. System A can ensure an irradiance value higher than 1kW/m$^2$, which is the approximated average irradiance at sea level on a clear sky day, while System B can only reach 0.64kW/m$^2$. In both solutions, the irradiance level can be adjusted since the bulbs in use are dimmable.

**Table 2.8.** Main characteristics of the solar simulation system solutions proposed by *Hönle*.

| | Type of light source | Number of lamps | Power consumed per lamp [kW] | Average flux [kW/m$^2$] | Homogeneity [%] | Light source to the testing surface distance [m] | Testing surface area [m$^2$] |
|---|---|---|---|---|---|---|---|
| **System A** | Metal Halide lamps | 4 | 4 | 1.07 | 92 | 1.5 | 2 |
| **System B** | Metal Halide lamps | 4 | 2.5 | 0.64 | 92 | 1.5 | 2 |

Moreover, both the luminaries are meant to be mounted vertically, in a way that the radiation beams are perpendicular to the athlete's height/body, 1.5m away from them. The irradiated surface is 2m wide and 1m long. This configuration was chosen so that the largest possible area of the athlete's body can be exposed to the same amount of radiation, since, unlike natural solar irradiance, which at earth's surface is approximately uniform throughout space, irradiance from solar simulators vary significantly with the distance.

The components of each system are: four HMI[12] 4000W double-ended or four HMI 2500W double-ended by *Osram*, for System A and System B, respectively; four lamp housings with extruded profile and aluminum sheets (reflectors); four brackets (for the floodlights); four EPSA (Electronic Power Supply) by *Hönle*; four built-in ignitors; four outdoor-spectrum filter-glass H2; and four cables. The overall price of one of the presented systems is roughly higher than 15k€. Figure 2.7 (a) shows a visual representation of one luminary (lamp, lamp housing and integrated ignitor).

*Sanwood* provides a different solar simulator system, which ensures an irradiance value of 1kW/m$^2$ at a distance of approximately 1.2m, with a metal halide lamp as its light source. *Sanwood* solution is presented in Figure 2.7 (b) and it consists of a ceiling mounted luminary composed by: one HMI 4000W/SE lamp by *Osram*, and its cover; one UV Glass-filter; one electronic power supply; one pyranometer; and one controller (Sanwood does not allow the purchase of these components separately). The set's overall price is 24,615 US$.

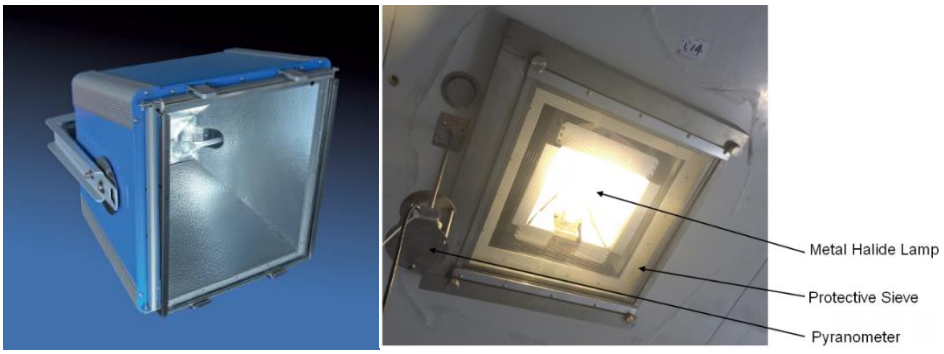


**Figure 2.7 a)** *Floodlight SFL* by *Hönle*, from the product catalog (Honle, n.d.) **b)** *Sanwood Solar Simulator for athlete training or material testing* (Sanwood, n.d.).

[12] HMI – Hydrargyrum medium arc iodide lamp (trademark name of *Osram*'s brand of metal halide gas discharge medium arc length lamp)

# 3. DESIGN OF THE SOLAR SIMULATOR

This chapter is dedicated to the design study of a solar simulator to improve the acclimation of high-performance athletes in LAI's climate chamber. This work focuses on the composition of one luminaire, the number of luminaires and their most adequate spatial configuration. The methodology followed to determine the optimal design is presented in the Figure 3.1.

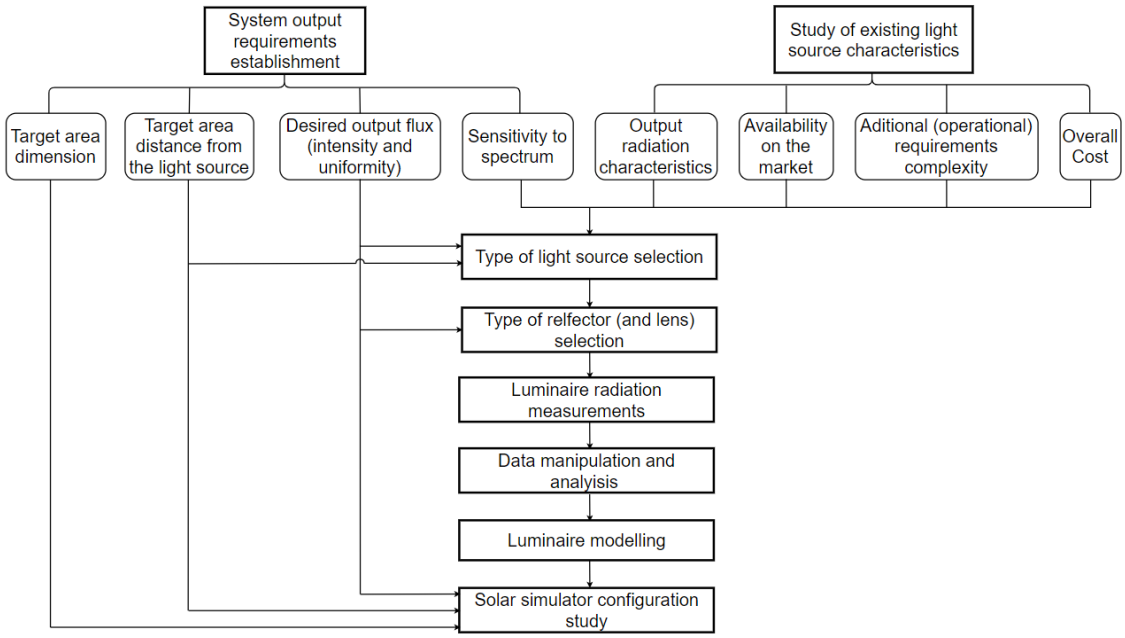


**Figure 3.1** Methodology followed to determine the solar simulator optimal design, adapted from (Tawfik et al., 2018).

## 3.1. System requirements and luminaire components selection

The first step in the design of any solar simulator system must be the definition of its requirements, followed by the selection of the type of light source that best fits the requirements (since it is the most crucial element of solar simulators).

### 3.1.1. System requirements

The solar simulator to be designed is to be used in acclimation training, therefore, its aim is to replicate the solar radiation at the athlete's training site. Since the dimensions of an average man are 1.88m in height and 0.4m in shoulder width (Singh et al., 2016), this study will consider a target area with a height of 2m and a width of 0.5m.

Furthermore, the solar radiation irradiance is approximately uniform on the earth's surface and, on a clear sky day, a total maximum irradiance value of 1000W/m$^2$ can be reached. It is aimed that the solar simulator to be designed in this work should be able to produce irradiance values of 800W/m$^2$, while providing a reasonable percentage of uniformity over the target area. A value of 70%, should be attained.

The distance from the light source is another aspect to be considered, since radiation intensity decreases drastically with the increase of the distance. This study will adopt a minimal distance between the target area and the light source of 1.25m, because it is believed to be the shortest possible distance to place the light source without disturbing the athlete.

In addition to irradiance level, the incident radiation spectrum also has an impact on athletes' performance, therefore the spectral match quality of the light source to be chosen must be a factor to be considered in the selection of the light source.

### 3.1.2. Type of light source selection

This selection is based on the information complied in the subchapters 2.2.3 and 2.2.4 . So, in this subchapter, one of the four common types of light sources (Xenon arc lamp, Quartz tungsten halogen lamp, Metal halide lamp and LED) is chosen by the exclusion of the others.

By analyzing the advantages and drawbacks listed in the Table 2.2, one can conclude that, although they are the most efficient light source and they have a great spectral match, LEDs alone are not a suitable choice of light source due to their low radiation intensity (the level of irradiance required would not be achieved). This fact is substantiated by the reading of Table 2.6 and Table 2.7, where it can be noticed that the vast majority of solar simulators that uses LEDs as their light source only attain high levels of radiation with the target surface at a small distance from the light source.

Halogen lamps have the advantages of being inexpensive, requiring a simple power supply and having the ability to hit high levels of irradiance at a considerable distance from the light source (as it can be seen in Table 2.4). Still, the author considers them to not be a good fit due to their poor spectral match quality in the UV and VIS ranges, their short lifetime, and the fact that many countries are ceasing their production with the growth of the LED industry.

Xenon arc lamps and Metal halide lamps are two types of gas discharge lamps. Both have a spectrum that closely matches the sun's spectrum and are relatively expensive. Xenon arc lamps have slightly better spectrum matches but they require a more complex and expensive power supply. By comparing the typical emission spectrums of the two lamps (Figure 2.3 and Figure 2.5) one can see the peak of radiation in the IR range is more significant in Xenon lamps, which may lead to a greater need for filtering. The reading of the overview of previous solar simulators used in human related studies allows one to realize that Metal halide lamps are the preferred type of light source. For all the reasons presented above, the author concludes that the best fit to the set requirements are the Metal halide lamps.

### 3.1.3. Type of reflector (and lens)

Reflectors and lenses are meant to redirect light beams. Parabolic reflectors and Fresnel lenses can be used as concentrators or collimators, and they are frequently seen in solar simulators. Figure 3.2 shows a scheme of both light redirection devices.

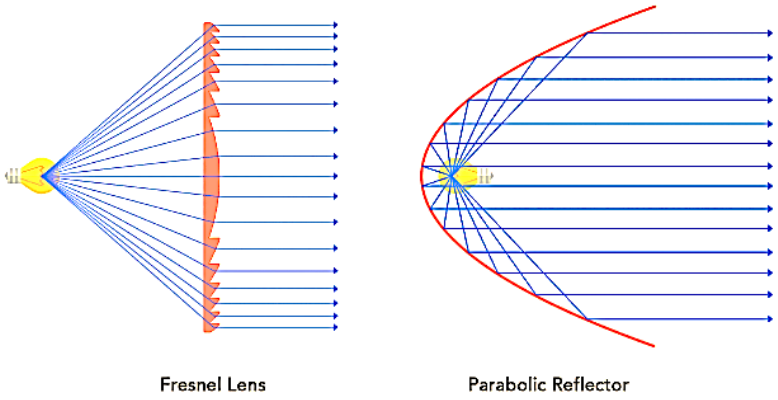


**Figure 3.2** Light collimation with a Fresnel Lens and a Parabolic reflector (Parabolix, n.d.).

To better fulfill the uniformity requirement, it's favorable that the target surface is hit by parallel beams. For this purpose, a Parabolic reflector is selected and a Fresnel is suggested, for each lamp.

## 3.2. Radiation Measurements

### 3.2.1. Purpose of the radiation measurements

In order to know how many luminaires are necessary to fulfill the established requirements, and in which position, a simulation study must be conducted.

Most of the available computer software aimed to study radiation of luminaires, only has the light calculation functionality, that is, only do calculations in the visible range of the spectrum. Thus, they only present results in photometric units (radiation units that are weighted according to the sensitivity of the human eye). Moreover, the manufacturers of lamps and light emitting devices only provide information about the photometric characteristics of their products. For example, it is common to see in a lamp data sheet its luminous efficacy, that is the amount of lumen produced in each watt consumed by the lamp, but it is never given the ratio between the number of watts radiated by each watt consumed.

To enable the use of a lighting design software in the dimensioning of the solar simulator, a conversion factor between the photometric units and radiometric units is needed (Michael et al., 2020). Since each wavelength has its own radiant flux value (radiant power), the conversion factor varies with the spectrum, thus, there is no general conversion factor that can be used in all lamps, and even lamps of the same type can have significantly different spectrums. To determine the conversion factor to be used in the interpretation of the software results, a pyranometer and a luxmeter were used to measure the emitted radiation of a luminaire integrated into an existing solar simulator.

### 3.2.2. Equipment, procedure method and measurements results

The measured luminaire's solar simulator belongs to Technological Center of Ceramics and Glass (CTCV[13]) of Coimbra. This solar simulator is used to test photovoltaic modules and solar thermal panels. The luminaires are composed by a metal halide lamp (*MSR 575 HR 1CT, Philips*), a parabolic reflector and a Fresnel lens, which corresponds to the planned design of this work solar simulator's luminaires. In addition, CTCV's solar simulator also had a ventilated double glass layer between the luminaires and the photovoltaic panel to filter the IR peak of radiation, but the measurements were made without the glass.

In twenty-four different points, the values of irradiance ($E_e$ in radiometric units: $W/m^2$) and of illuminance ($E_v$ in photometric unis: lx[14]) were measured through the use of a pyranometer (*Smp11-A, Kipp & Zonen*) and a luxmeter-colormeter (*C-800 SpectroMater*

[13] CTCV – *Centro Tecnológico da Cerâmica e do Vidro*.
[14] $lx = lm/m^2$

*Color Meter*, *Sekonic)*, respectively. Each meter was attached to a tripod for ease of positioning, as shown in Figure 3.3.

**Figure 3.3** Photo of the *Smp11-A pyranometer* and the *C-800 SpectroMaster Color Meter*.

As the luminaire is expected to emit symmetrically in all directions (due to its geometry), the measurement points were spatially distributed according to the Figure 3.4 (b).

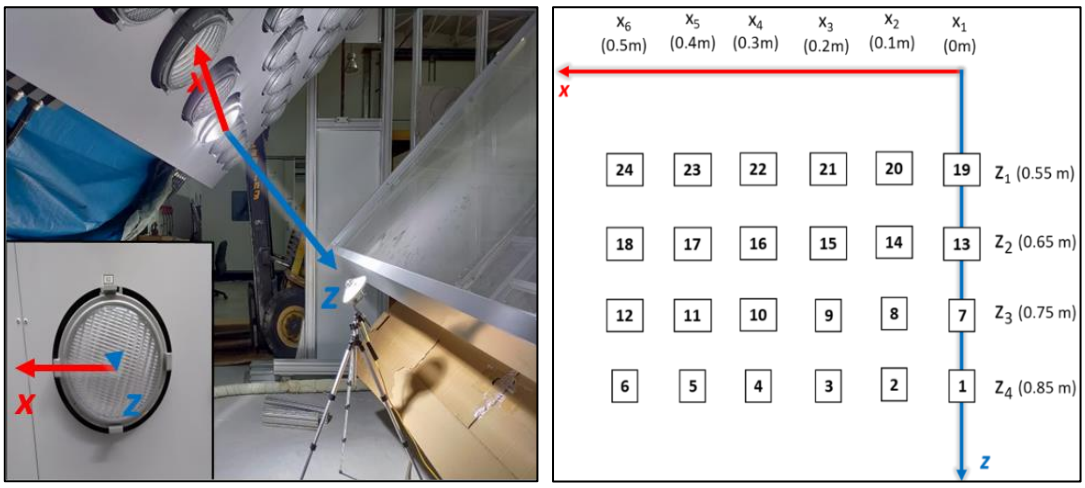


**Figure 3.4 a)** 3D visualization of the considered measurements axes **b)** 2D visualization of the measuring points in relation to the axes (not to scale).

The measurements were made with the meters placed parallel to the plane where the luminaire was located, rather than towards the luminaire, for ease of positioning. Therefore, it becomes necessary to correct the measuring results according to the angle between the light beam and the perpendicular vector to the meter. The corrected measurements results are presented in the Table 3.1 and in the Figure 3.5.

**Table 3.1.** Corrected measurements Results

| | Units | X6 (0.5m) | X5 (0.4m) | X4 (0.3m) | X3 (0.2m) | X2 (0.1m) | X1 (0m) |
|---|---|---|---|---|---|---|---|
| **Z1 (0.55m)** | lx | 5906 | 8507 | 15036 | 40222 | 109771 | 146000 |
| | W/m$^2$ | 62 | 93 | 151 | 385 | 1066 | 1160 |
| **Z2 (0.65m)** | lx | 5564 | 8501 | 13216 | 37561 | 87315 | 105000 |
| | W/m$^2$ | 58 | 92 | 156 | 368 | 745 | 1033 |
| **Z3 (0.75m)** | lx | 4988 | 7797 | 15617 | 36637 | 70821 | 78800 |
| | W/m$^2$ | 62 | 88 | 126136 | 338 | 613 | 789 |
| **Z4 (0.85m)** | lx | 5209 | 8167 | 15165 | 34723 | 54372 | 61100 |
| | W/m$^2$ | 61 | 76 | 170 | 321 | 520 | 583 |

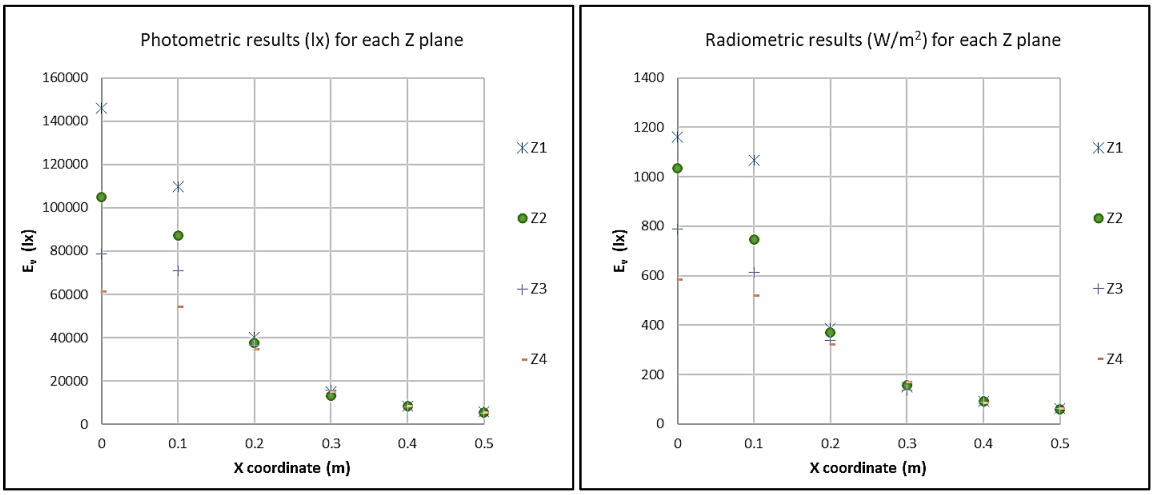


**Figure 3.5** Graphic representation of the corrected measurements results: **a)** in photometric units **b)** in radiometric units.

It is important to refer that the conditions in which the measurements were taken were not ideal. The room, where the measurements took place, was illuminated by other light sources, yet their influence on the measurements is thought to be negligible.

The meters were carefully positioned in each spatial point using a measuring tape. The error associated with positioning is ± 0.005m. The accuracy of the illuminance measurements of *C-800 SpectroMater Color Meter* is ± 5% and the accuracy of the irradiance measurements of S*mp11-A* pyranometer is ± 0.2 %. Furthermore, unlike the luxmeter used, which measures instantaneously, the pyranometer used was measuring continuously. The measured values were being displayed on a screen and were varying very slightly. The readed values were then annoted. Due to this minor variation, the accuracy of the irradiance measured values is expected to narrowly exceed 0.2%.

In addition to illuminance measurements, the *C-800 SpectroMater Color Meter* also measured the emitted spectrum. Figure 3.6 shows the spectrum measurement of the studied luminaire and of the sun in a clear sky day.

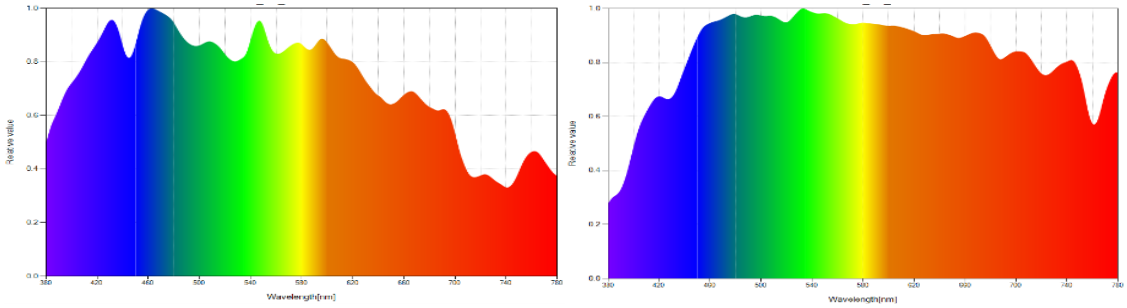

Figure 3.6 Spectrum measurements of a) the studied luminaire b) the sun in a clear sky day.

## 3.3. Data analysis and manipulation

### 3.3.1. Measurements results interpolation

In pursuance of modeling the luminaire more precisely, it is important to obtain an approximation of the irradiance and illuminance values between the measured points. That can be accomplished through interpolations, using *Excel* trend lines.

By observing Figure 3.5, for every plane Z, one can see two different behaviors in the evolution of illuminance and the evolution of irradiance with the coordinate $X$. The reason for this is thought to be that the points after $X3$ may not be affected directly by the main light cone. Taking this into account, two trend lines were drawn for each Z plane, as shown in Figure 3.7.

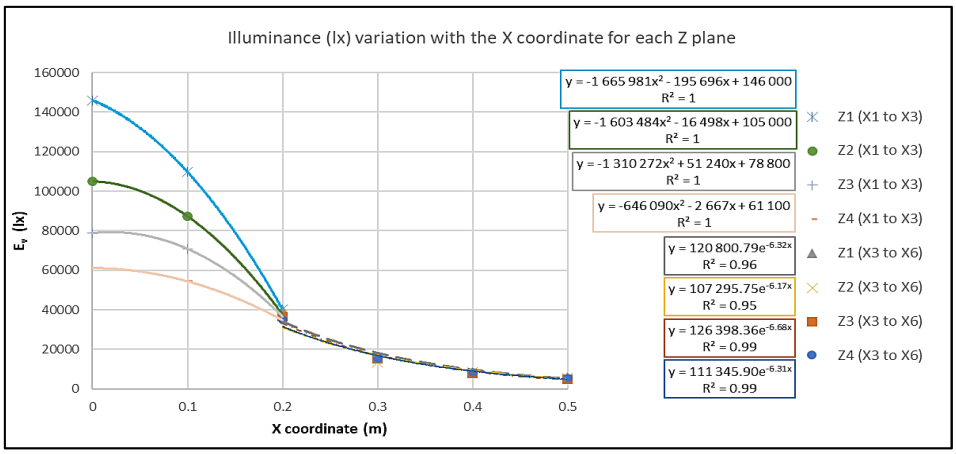

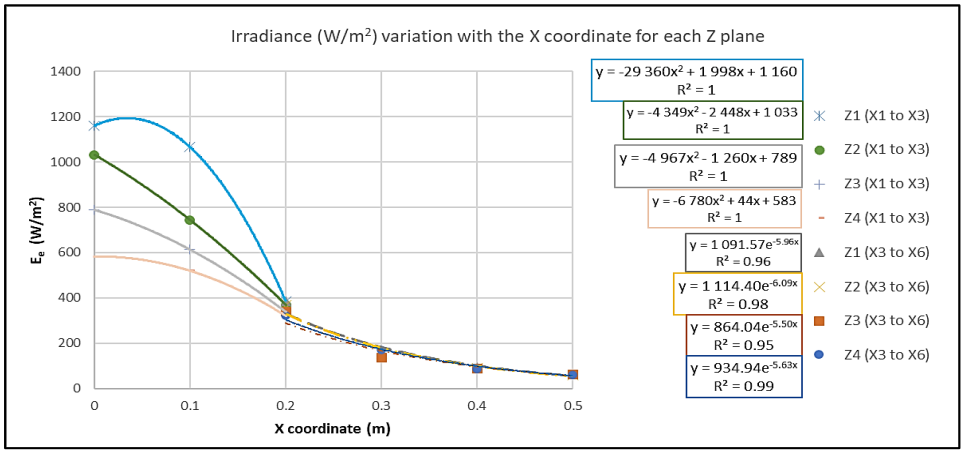


**Figure 3.7** Trend lines of the measurements results: **a)** in photometric units **b)** in radiometric units.

Below the equations of the trend lines, their coefficients of determination are shown. All trend lines present a coefficient close to 1, which indicates strong correlations. Nonetheless, due to the small number of measured points, the curves referring to *(X1 to X3)* are overfitting. The accuracy of these curves could be increased if more measurements were taken between the points.

## 3.3.2. Beam angle calculation

Beam angle is defined as the angle between two opposed directions over the beam axis (Z axis, in the present work) for which the luminous intensity is half of the maximum luminous intensity (Lamp HQ, n.d.). The beam angle determines the dimension of the generated light circle on the illuminated plane. A visual explanation of the concept of beam angle can be found in Figure 3.8. Theoretically, the result of beam angle calculation does not depend on which plane the values used in the calculation were taken from, nor if the values are the photometric or the radiometric ones. With that in mind, the beam angle was determined, with the photometric values, for the four Z planes. The average of the four results was considered the final value.

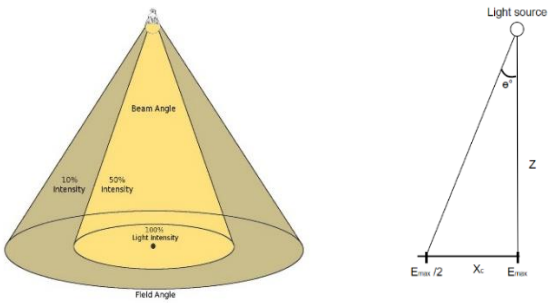


**Figure 3.8** **a)** Visual explanation of the beam angle concept (Lamp HQ, n.d.) **b)** scheme of the calculations.

The first step of the calculation is the determination of $X_C$ (represented on Figure 3.8). $X_C$ represents the $X$ coordinate for which the light intensity value corresponds to half of the maximum light intensity measured on the plane. With this aim, the trend lines equations were manipulated in order to determine $X$ coordinate. Equation 3.1 shows the generic manipulation of both types of trend lines functions.

$$\begin{cases} for\ \ X1\ to\ X3\text{: } y = aX^2 + bX + c \\ \quad for\ \ X3\ to\ X6\text{: } y = ae^{-bX} \end{cases} \Leftrightarrow \begin{cases} X = \dfrac{-b \pm \sqrt{b^2 - 4a(c-y)}}{2a} \\ X = -\dfrac{\ln({}^{y}/_{a})}{b} \end{cases} \quad (3.1)$$

Where $y$, in this case, represents half of the maximum measured illuminance ($E_{v,maximum}$ /2 in lx).

In planes Z1, Z2 and Z3, the half of the maximum illuminance was located between the values measured at $X2\ to\ X3$, so $X_C$ was calculated with the function for $X1\ to\ X3$. In Z4 plane, $X_C$ was calculated with the function for $X3\ to\ X6$. The conclusion that the value of $X_C$ is inferior and close to the value of $X3$ supports the previous speculation that data with an $X$ coordinate above $X3$ may not be directly affected by the generated main light cone.

With the knowledge of $X_C$ value, the beam angle values for each plane were estimated by means of Equation 3.2 and Equation 3.3.

$$\Theta = \tan^{-1}({}^{X_C}/_{Z}), \quad (3.2)$$

$$Beam\ Angle\ = 2\Theta \quad (3.3)$$

The average estimated $Beam\ Angle$ is 29.69 °.

### 3.3.3. Irradiance-Illuminance conversion

As to calculate the irradiance-illuminance conversion factor and to modeling the luminaire, the conversion of the data to polar coordinates is required. With increments of 3º, and from 0 ° to 87°, the radiometric and the photometric values were determined, for each Z plane. Firstly, the $X$ coordinate correspondent to each Θ and Z plane was obtained by using Equation 3.4. Secondly, with the value of $X$ known, the functions of the trend lines were applied to estimate the associated values of irradiance and illuminance. The choice of which trend line to use was made by checking between which intervals the $X$ value was inserted, $X1\ to\ X3$ or $X3\ to\ X6$.

$$X = \mathrm{Z} \tan \theta, \tag{3.4}$$

To calculate the irradiance-illuminance conversion factor of the studied lumianaire, the quotients of illuminance and irradiance were obtained from 0° to 30° (which approximately corresponds to the estimated beam angle). The average of these quotients was adopted as the conversion factor: 1 W/m$^2$ =109.8lx.

Michael et al. (2020), conducted a similar study, in which the conversion factors for radiation from a *MiniSol* LED solar simulator and from natural solar radiation were calculated. The obtained conversion results were 1 W/m$^2$ =116 ± 3 lx and 1 W/m$^2$ =122 ± 1 lx, respectively.

## 3.4. Luminaire modeling

The software selected to conduct the solar simulator configuration study is *DIALux*. *DIALux* is an open and intuitive lighting design software that allows the import of custom luminaires. The formats of the luminaires files accepted by *DlALux* are IES, LDT and ULD. The first two formats can be created and edited by the user. LDT is an extended photometric which contains more information than a IES file, therefore it describes the luminaire more precisely. So, to import to *DIALux* the collected data, an LDT file must be edited using the *LDT Editor* software.

### 3.4.1. Modeling in *LDT Editor*

**Entered data**

An LDT file contains information about the luminaire housing and lamp characteristics, which were gathered from their datasheet. The following information was inserted into the software - Diameter of luminaire: 0.21m; Diameter of luminous area: 0.25m; Number of lamps: 1; Type of lamps: Metal Halide; Total luminous flux: 49000lm; Colour temperature: 6000K; Colour rendering index: 90; Connected power: 575W; Luminous intensities values, for each angle.

Luminous intensity ($I_v$) has candela (cd) as its unit. Luminous intensity can be calculated by the product of illuminance (lx) and the square of the distance from the light source (m$^2$) (CompuPhase, 2019). LDT photometry files work with the luminous intensity

values relative to the lamp's luminous flux, therefore their units are candela per kilolumen (cd/klm).

To insert this information in the *LDT Editor*, the illuminance data was, firstly, converted to polar coordinates. With increments of 3º, and from 0 ° to 87°, four illuminance values (in lux), one for each Z plane were determined, for each angle (θ). The distance of these new spatial locations from the light source was also calculated. Equation 3.5 uses these two known variables to calculate the luminous intensity (in candela) of each angle θ.

$$I_v = E_v \ d^2 \tag{3.5}$$

For the same angle, according to the inverse square law, the luminous intensity should not depend on which spatial point the data is referring to. However, due to errors, the results slightly differ from one another. Consequently, for each angle θ, the average of the four results was established as the value of luminous intensity. Figure 3.9 exhibits the scheme of these calculations, for a better understanding.

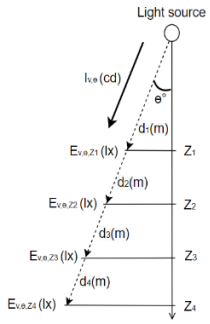


**Figure 3.9** Scheme of the light luminous intensity calculations.

The luminous intensities (in candela) were then divided by the lamp's total luminous flux, which is 49klm. It is important to notice that, as it ages, the lamp's luminous intensity tends to be reduced. The data sheet's indication of 49klm refers to the begining of use value. Thus, the values of luminous intensity values relative to the lamp's luminous flux may be faintly undersized.

At last, this data was entered into the software.

**Output data**

Besides creating an LDT file that can be imported into *DIALux*, *LDT Editor* also provides the user the luminaire's light distribution graphs and other technical information.

Luminaires' light distributions are commonly represented in polar curves. In other words, polar curves display the luminous intensity in all directions. Figure 3.10 shows the polar curve defined by the relative luminous intensities input values.

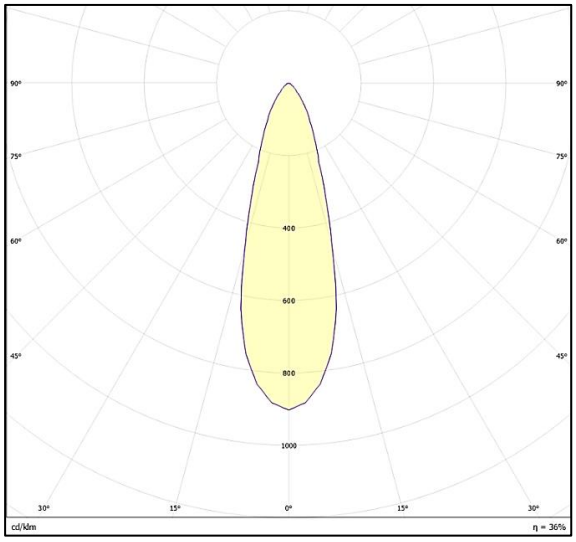


**Figure 3.10** Luminaire's polar curve.

*LDT Editor*'s calculated beam angle is 30.4° (which closely matches the estimated value of 29.69°). With the lamp's total luminous flux and the luminous intensities input values, the software also calculates the luminaire's efficiency (the light output ratio). The studied luminaire's efficiency is 36.42%.

The software still uses the lamp's total luminous flux, together with connected power, to calculate the luminous efficacy, which is 85.22lm/W (this information is also presented in the lamps data sheet).

### 3.4.2. Model validation

Since LDT files do not contain the lamp's spectrum data, once the file is imported into *DIALux* it assumes a default spectrum. The software has a set of standard spectrums of which was selected the one that most resembled the luminaire measured spectrum.

To validate the model created, the measurements' conditions were replicated in *DIALux*. In order to replicate the Z planes, four calculation surfaces were placed perpendicular to the light source (Figure 3.11 (a)). The simulated values of illuminance ($E_v$ in lux) in the Z1 plane are shown in Figure 3.11 (b). The beam axis (Z axis) is represented by the orange central dot, and the *X* coordinates are indicated by the auxiliary lines.

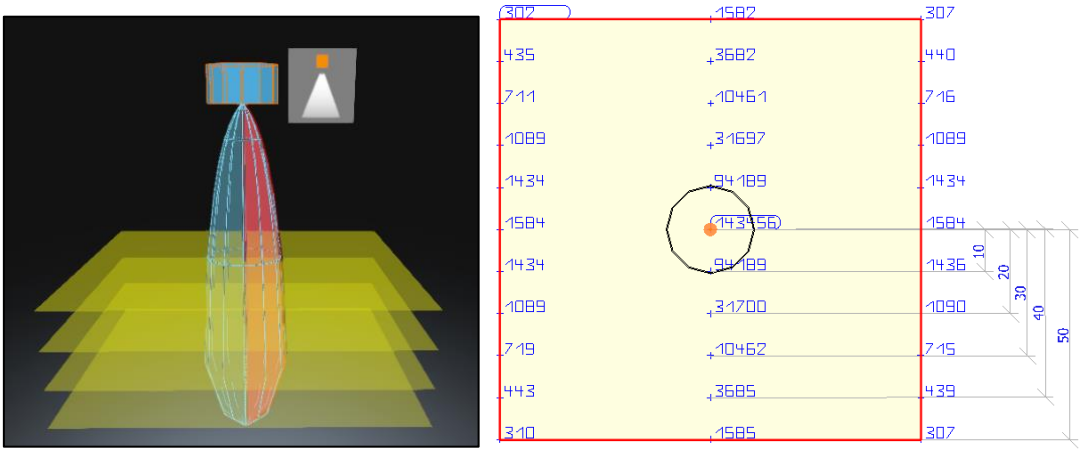


**Figure 3.11 a)** 3D representation of the measurement planes and luminaire's geometry and light distribution **b)**Simulated illuminance values in the Z1 plane.

For easier comparison, Figure 3.12 shows a graph containing the illuminance measured and simulated results variation with the X coordinate, for the Z1 plane. It is noticeable that the simulation curves indicate lower illuminance levels than the measured curves. The average absolute difference between the measured and the simulated values (of the four planes) is 4425.8lx, which is equivalent to 40.3W/m$^2$, for this luminaire. Some possible explanations for this difference are: underdimensioned luminaire's luminous intensities, due to the disregard of the lamp aging; the nonconsideration of the use of a parabolic reflector and a Fresnel lens by the luminaire model in *DIALux* (as it can be seen in Figure 3.11 (a)). The analysis of the remaining Z planes led to similar graphs and identical conclusions.

In conclusion, although there is no perfect match between the measurements and the simulation curves, their similarity points leads to the conclusion that the model is valid.

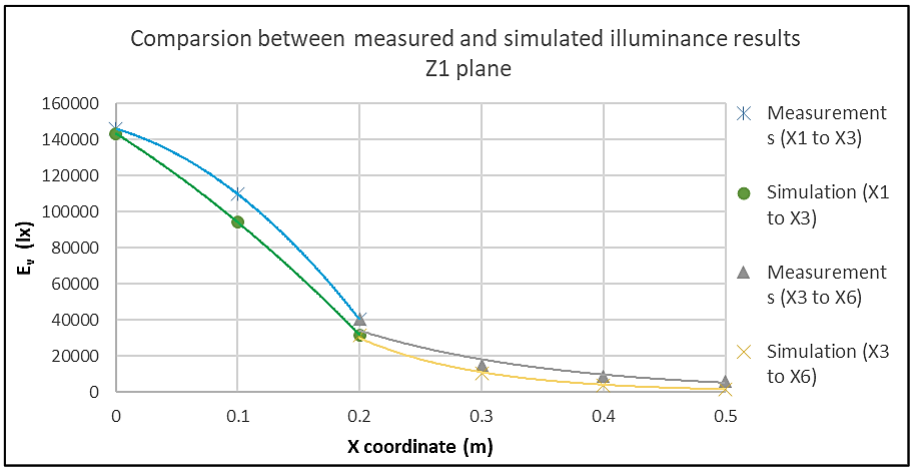

**Figure 3.12** Measured and simulated illuminance values variation in Z1 plane.

## 3.5. Solar simulator configuration study

### 3.5.1. LAI's climate chamber

The solar simulator is intended to be installed in LAI's climate chamber. This climate chamber is a wooden modular structure, composed by two compartments: the test chamber and the control chamber. The test chamber, as the name suggests, is where the trials take place. It is a roughly square shaped room with an area of approximately $23m^2$ and it has a movable ceiling that allows its heigh to vary between 2.1m and 4.8m. This chamber is equipped with four air handling units, sensors and a treadmill. The control chamber is the smallest room. It has an area of $16m^2$ and a fixed ceiling heigh of 2.8m and it contains the equipment to monitor and control the test chamber.

The teste chamber, the treadmill and an athlete using it were replicated in *DIALux*.

### 3.5.2. Configuration study

#### 3.5.2.1. Requirements

As stated in the subchapter 3.1.1, the requirements that the solar simulator has to fulfill are as follows:

1. Target area dimension: heigh of 2m and width of 0.5m.
2. Target area minimal distance from the light source: 1.25m.
3. Desired output flux: $800W/m^2$, with an uniformity index of 0.7.

Uniformity index ($u_0$) refers to the ratio between minimum illuminance and the average illuminance ($E_{v,\,min}$ / $E_{v,\,average}$). *DIALux* determines this property automatically.

In addition to these requirements, it is pertinent to add that the luminaires must be directed to the athlete's back, to prevent ocular injuries due to the lamp's high luminous intensity (i.e., intense brightness).

#### 3.5.2.2. Angle and positioning

In an attempt to meet these requirements, five configurations were studied. The number of luminaires and their spatial positioning differ in accordance with the configuration in question, whereas the luminaires' inclination angle remains unchanged.

The setting of the luminaires' inclination angles is meant to mimic the sun's inclination angle. So, the radiation from the solar simulator would hit the athlete the same way the natural solar radiation typically does. For this reason, its angle with the vertical takes the value of the solar zenith angle, which was considered as 60º. In all configurations, the luminaires were placed in the same plane and with the same orientation so that the resulting radiation of the setup is as parallel as possible (resembling sun's radiation).

#### 3.5.2.3. Configurations description

Configuration A consists of twelve luminaires distributed over two columns of six luminaires each. The luminaires' axes are 0.4m apart from one another and the overall set is 1.25m distant from the testing area. Figure 3.13 presents the visual description of Configuration A. The yellow rectangle represents the testing area.

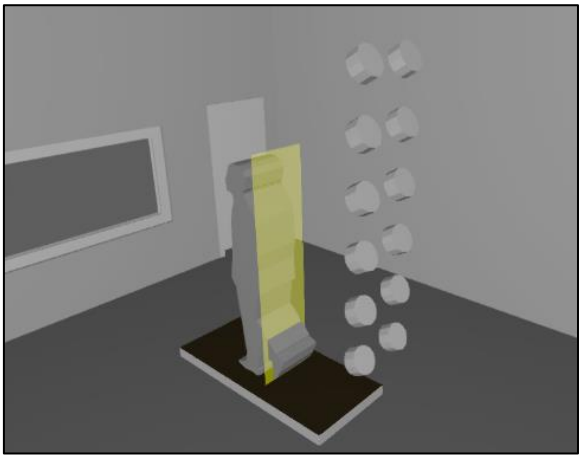

**Figure 3.13** Configurarion A's visual description.

Configuration B is in every way similar to Configuration A except the luminaires' axes are 0.3m apart from one another.

Configuration C differes from Configurations A and B in what comes to the number of luminaires and the distance between their axes. Configuration C has fourteen luminaires and their axes distance 0.35m vertically and 0.3m horizontally from one another.

In Configuration D the number of lumianires was increased to twenty-one. From Configuration C another column of seven luminaires was added. All the other characteristics remained the same.

Configuration E has the same characteristics as Configuration D, except that the overall set distance is 1.5m from the testing area.

#### 3.5.2.4. Results

The summary of the configurations' simulation results are presented in the Table 3.2.

**Table 3.2.** Simulations results of the five configurations.

| | $E_{v,\ average}$ (lx) | $E_{v,\ max}$ (lx) | $E_{v,\ min}$ (lx) | $E_{e,\ average}$ ($W/m^2$) | $E_{e,\ max}$ ($W/m^2$) | $E_{e,\ min}$ ($W/m^2$) | $u_0$ (-) | Nº of luminaires |
|---|---|---|---|---|---|---|---|---|
| **Configuration A** | 62490 | 70846 | 38972 | 569.1 | 645.2 | 354.9 | 0.62 | 12 |
| **Configuration B** | 79740 | 106034 | 34108 | 726.2 | 965.7 | 310.6 | 0.43 | 12 |
| **Configuration C** | 79604 | 93405 | 54009 | 725.0 | 850.7 | 491.9 | 0.68 | 14 |
| **Configuration D** | 100681 | 109091 | 83897 | 916.9 | 993.5 | 764.1 | 0.83 | 21 |
| **Configuration E** | 88016 | 97423 | 70434 | 801.6 | 887.3 | 641.5 | 0.8 | 21 |

The irradiance ($E_e$) values were established through the use of the conversion factor 1 $W/m^2$ =109.8lx, calculated in the subchapter 3.3.3. The values of illuminance ($E_v$) and uniformity index ($u_0$) were provided by *DIALux*. In reality, slightly higher values of illuminance and irradiance are expected because the lamp's model is thought to be also narrowly undersized, as Figure 3.12, in the subchapter 3.4.2, illustrates. Figure 3.14 shows the false color rendering results on the testing area, of the five configurations.

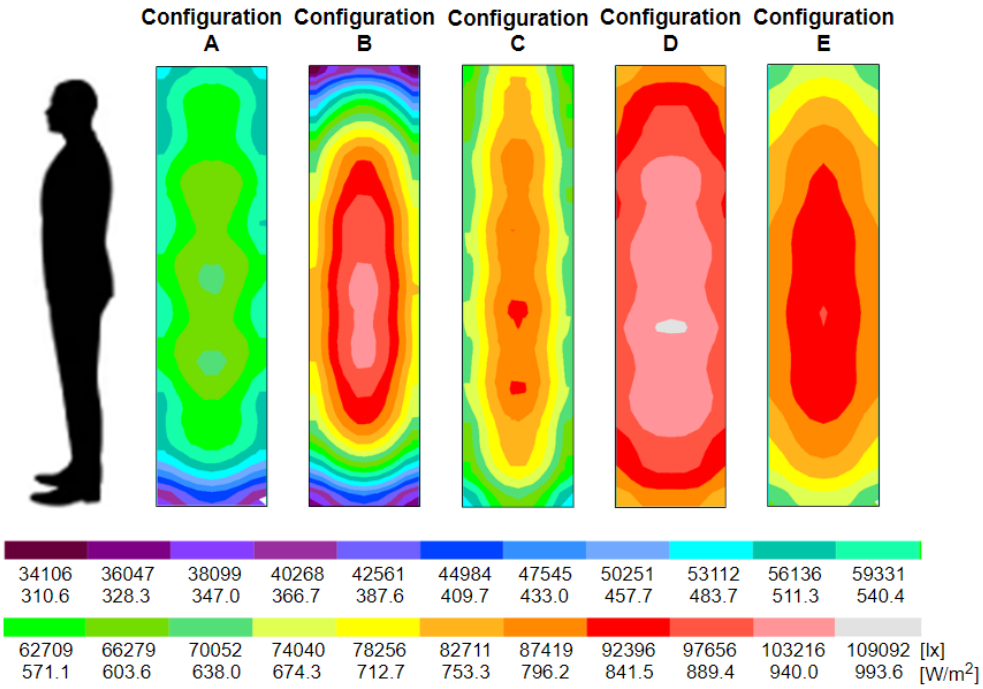


**Figure 3.14** False colour rendering results on the test area, of the studied configurations.

By analyzing the results displayed in Figure 3.14 and Table 3.2, one can conclude that increasing the number of luminaires not only implies increasing the value of irradiance, but also the uniformity value. In contrast, increasing the axes' distance from one another entails decreasing the value of irradiance, but also the uniformity value

All configuration' over all luminaires sets are at least 1.25 distant from the testing area.

In all configurations except Configuration A, the irradiance average values are higher than 700W/m$^2$. In Configurations D and E, the average irradiance exceeds 800W/m$^2$.

In configurations C, D and E the uniformity value is either close to the required value or exceeds it.

Configurations D and E fulfill all the set requirements. Configuration E has lower values of uniformity and irradiance but it is farthest from the athlete, which can be advantageous. Nevertheless, Configuration D was selected.

Configuration C's average irradiance and uniformity index are relatively close to the set requirements. If the set requirements were slightly lowered, this configuration would appear to be a better solution than Configurations D and E, as it has smaler number of

luminaires. Since the model is thought to be narrowly undersized, it is possible that in reality Configuration C can achieve an average irradiance value higher than 800W/$m^2$.

In addition, although its uniformity index is low, Configuration B causes a large area of the athlete's back to be under a value of irradiance greater than 800W/$m^2$, as Figure 3.14 shows.

To summarize, Configuration D was selected because it is the configuration that presents the most promising results ($u_0$ = 0.83 and $E_{e,\ average}$ = 916.9W/$m^2$).

# 4. CONCLUSIONS

The motivation behind the realization of this study was the improvement of high performance athletes' acclimation training. The purpose of this work was to study and design a solar simulator to upgrade LAI's climate chamber simulation capacities. In this sense, this work was divided into two sections. First section: the solar simulators' state of art summary, which allowed the author to learn which was the most appropriate technology to be employed, considering the main goal. Second section: the solar simulator configuration study, resorting to *DIALux*.

The light source chosen for the designed solar simulator was a metal halide lamp. To redirect the light beams, a parabolic reflector was also selected and a Fresnel lens was suggested.

Through radiation measurements and mathematical manipulations, a model of the studied luminaire was created in *DIAlux*. The model has proven that it can replicate well the characteristics of the real luminaire, even being slightly undersized. The existing inaccuracies are associated with the measurement data and the interpolated values. To be able to interpret *DIALux* results in radiometric units, an illuminance-irradiance conversion factor was determined.

The resulting value was very similar to the conversion factor for natural solar radiation, calculated in a previous paper (Michael et al., 2020). Five configurations were studied with *DIALux*. Of these five, two configurations were able to fulfill the set requirements. Configuration D presented the best results: 21 luminaires; 1.25m distant from the testing area; uniformity index of 0.83; average irradiance value of 916.9 $W/m^2$; maximum irradiance value of 993.5 $W/m^2$.

One suggestion for improving the quality of the model is to increase the number of measuring points, so that the approximations based on them can be more accurate. A further suggestion for improving this work is the modeling of different luminaires, with different lamp power and different housing, so a wider variety of configurations could be studied. During the course of this work, a system of LED luminaires was also defined and installed (in the climate chamber), which will allow future studies of the athletes' circadian cycle.

Finally, the author concludes that Configuration D's solar simulator would contribute significantly to the improvement of athletes' acclimation training. Besides that, because the lamps' spectrum is similar to the sun's spectrum, the athletes' production of melatonin could be affected. Thus, prolonged exposure may impact their circadian cycles. As the results of this study show that is possible to sufficiently reproduce the effect of solar radiation on an athlete, future work would be the acquisition and installation of the designed system.

# BIBLIOGRAPHY

Bliss, M., Betts, T. R., & Gottschalg, R. (2009). An LED-based photovoltaic measurement system with variable spectrum and flash speed. *Solar Energy Materials and Solar Cells*, *93*(6–7), 825–830. https://doi.org/10.1016/j.solmat.2008.09.056

Bodnár, I., Koós, D., Iski, P., Skribanek, Á., & Machinery, C. (n.d.). Design and Construction of a Sun Simulator for Laboratory Testing of Solar Cells. In *Acta Polytechnica Hungarica* (Vol. 17, Issue 3).

Codd, D. S., Carlson, A., Rees, J., & Slocum, A. H. (2010). A low cost high flux solar simulator. *Solar Energy*, *84*(12), 2202–2212. https://doi.org/10.1016/j.solener.2010.08.007

Colarossi, D., Tagliolini, E., Principi, P., & Fioretti, R. (2021). Design and Validation of an Adjustable Large-Scale Solar Simulator. *Applied Sciences*, *11*(4), 1964. https://doi.org/10.3390/app11041964

CompuPhase. (2019). *Candela, Lumen, Lux: the equations*. Https://Www.Compuphase.Com/Electronics/Candela_lumen.Htm#APEX_ANGLE.

Dai, S., Chang, Z., Ma, T., Wang, L., & Li, X. (2019). Experimental study on flux mapping for a novel 84 kWe high flux solar simulator. *Applied Thermal Engineering*, *162*, 114319. https://doi.org/10.1016/j.applthermaleng.2019.114319

Deepak, Srivastava, S., & Malvi, C. S. (2020). Light sources selection for solar simulators: A review. *WEENTECH Proceedings in Energy*, 28–46. https://doi.org/10.32438/wpe.060257

Dionísio, F. (2021). *DESENVOLVIMENTO E TESTE DE MODELOS DE CONTROLO DO SISTEMA DE CLIMATIZAÇÃO DE UMA CÂMARA CLIMÁTICA*. Universidade de Coimbra.

Dutta Gupta, S., & Agarwal, A. (2017). Artificial Lighting System for Plant Growth and Development: Chronological Advancement, Working Principles, and Comparative Assessment. In *Light Emitting Diodes for Agriculture* (pp. 1–25). Springer Singapore. https://doi.org/10.1007/978-981-10-5807-3_1

Esen, V., Sağlam, Ş., & Oral, B. (2017). Light sources of solar simulators for photovoltaic devices: A review. In *Renewable and Sustainable Energy Reviews* (Vol. 77, pp. 1240–1250). Elsevier Ltd. https://doi.org/10.1016/j.rser.2017.03.062

Foster, J., Smallcombe, J. W., Hodder, S., Jay, O., Flouris, A. D., Nybo, L., & Havenith, G. (2022). Quantifying the impact of heat on human physical work capacity; part III: the impact of solar radiation varies with air temperature, humidity, and clothing coverage. *International Journal of Biometeorology*, *66*(1), 175–188. https://doi.org/10.1007/s00484-021-02205-x

G2V Optics. (n.d.). *A guide to solar simulation and solar simulators*. Retrieved August 11, 2022, from https://g2voptics.com/solar-simulation/

Gallo, A., Marzo, A., Fuentealba, E., & Alonso, E. (2017). High flux solar simulators for concentrated solar thermal research: A review. *Renewable and Sustainable Energy Reviews*, *77*, 1385–1402. https://doi.org/10.1016/j.rser.2017.01.056

Grandi, G., Ienina, A., & Bardhi, M. (2014a). Effective Low-Cost Hybrid LED-Halogen Solar Simulator. *IEEE Transactions on Industry Applications*, *50*(5), 3055–3064. https://doi.org/10.1109/TIA.2014.2330003

Grandi, G., Ienina, A., & Bardhi, M. (2014b). Effective Low-Cost Hybrid LED-Halogen Solar Simulator. *IEEE Transactions on Industry Applications*, *50*(5), 3055–3064. https://doi.org/10.1109/TIA.2014.2330003

Hodder, S. G., & Parsons, K. (2006). The effects of solar radiation on thermal comfort. *International Journal of Biometeorology*, *51*(3), 233–250. https://doi.org/10.1007/s00484-006-0050-y

Honle. (n.d.). *Product information Solar Simulation Floodlight SFL*. Https://Www.Hoenle.Com/Hoenle.de/Pdfs/Produktbroschueren/En/Solar-Simulator-Floodlight-Sfl.Pdf.

Irwan, Y. M., Leow, W. Z., Irwanto, M., Fareq.M, Amelia, A. R., Gomesh, N., & Safwati, I. (2015). Indoor Test Performance of PV Panel through Water Cooling Method. *Energy Procedia*, *79*, 604–611. https://doi.org/10.1016/j.egypro.2015.11.540

Jin, J., Hao, Y., & Jin, H. (2019). A universal solar simulator for focused and quasi-collimated beams. *Applied Energy*, *235*, 1266–1276. https://doi.org/10.1016/j.apenergy.2018.09.223

Kim, K. A., Dostart, N., Huynh, J., & Krein, P. T. (2014). Low-cost solar simulator design for multi-junction solar cells in space applications. *2014 Power and Energy Conference at Illinois (PECI)*, 1–6. https://doi.org/10.1109/PECI.2014.6804544

Klous, L., de Ruiter, C., Alkemade, P., Daanen, H., & Gerrett, N. (2020). Sweat rate and sweat composition during heat acclimation. *Journal of Thermal Biology*, *93*, 102697. https://doi.org/10.1016/J.JTHERBIO.2020.102697

Ko, Y., Kang, J., Seol, S. H., & Lee, J. Y. (2020). Effectiveness of skin-heating using a water-perfused suit as passive and post-exercise heat acclimation strategies. *Journal of Thermal Biology*, *93*, 102703. https://doi.org/10.1016/J.JTHERBIO.2020.102703

Lamp HQ. (n.d.). *LED Beam Angle Guide – With Beam Angle Calculator*. Https://Lamphq.Com/Beam-Angle/#explanation-of-Led-Beam-Angle.

Li, X., Chen, J., Lipiński, W., Dai, Y., & Wang, C.-H. (2020). A 28 kWe multi-source high-flux solar simulator: Design, characterization, and modeling. *Solar Energy*, *211*, 569–583. https://doi.org/10.1016/j.solener.2020.09.089

Lucas-Sánchez, A., Martinez-Nicolas, A., Escames, G., & de Costa, J. (2012). Envejecimiento del sistema circadiano. In *Revista Espanola de Geriatria y Gerontologia* (Vol. 47, Issue 2, pp. 76–80). Ediciones Doyma, S.L. https://doi.org/10.1016/j.regg.2011.09.008

Mahmoud Shatat. (2013). *Experimental testing method for solar light simulator with an attached evacuated solar collector*.

Martínez-Manuel, L., Peña-Cruz, M. I., Villa-Medina, M., Ojeda-Bernal, C., Prado-Zermeño, M., Prado-Zermeño, I., Pineda-Arellano, C. A., Carrillo, J. G., Salgado-Tránsito, I., & Martell-Chavez, F. (2018). A 17.5 kWel high flux solar simulator with controllable flux-spot capabilities: Design and validation study. *Solar Energy*, *170*, 807–819. https://doi.org/10.1016/j.solener.2018.05.088

Mei, L., Infield, D. G., Gottschalg, R., Loveday, D. L., Davies, D., & Berry, M. (2009). Equilibrium thermal characteristics of a building integrated photovoltaic tiled roof. *Solar Energy*, *83*(10), 1893–1901. https://doi.org/10.1016/j.solener.2009.07.002

Meng, Q., Wang, Y., & Zhang, L. (2011). Irradiance characteristics and optimization design of a large-scale solar simulator. *Solar Energy*, *85*(9), 1758–1767. https://doi.org/10.1016/j.solener.2011.04.014

Michael, P. R., Johnston, D. E., & Moreno, W. (2020). A conversion guide: solar irradiance and lux illuminance. *Journal of Measurements in Engineering*, *8*(4), 153–166. https://doi.org/10.21595/jme.2020.21667

Namin, A., Jivacate, C., Chenvidhya, D., Kirtikara, K., & Thongpron, J. (2012). Construction of Tungsten Halogen, Pulsed LED, and Combined Tungsten Halogen-

LED Solar Simulators for Solar Cell <math> <mi>I</mi> </math> - <math> <mi>V</mi> </math> Characterization and Electrical Parameters Determination. *International Journal of Photoenergy*, *2012*, 1–9. https://doi.org/10.1155/2012/527820

NASA, U. Gov. (1974). *A low cost "'Air Mass 2'''' solar simulator.'"*

Ööpik, V., Timpmann, S., Kreegipuu, K., Unt, E., & Tamm, M. (2014). Heat acclimation decreases the growth hormone response to acute constant-load exercise in the heat. *Growth Hormone & IGF Research*, *24*(1), 2–9. https://doi.org/10.1016/J.GHIR.2013.10.001

Otani, H., Kaya, M., Tamaki, A., Goto, H., Tokizawa, K., & Maughan, R. J. (2021). Combined effects of solar radiation and airflow on endurance exercise capacity in the heat. *Physiology & Behavior*, *229*, 113264. https://doi.org/10.1016/j.physbeh.2020.113264

Otani, H., Kaya, M., Tamaki, A., Hosokawa, Y., & Lee, J. K. W. (2020). Solar radiation and the validity of infrared tympanic temperature during exercise in the heat. *International Journal of Biometeorology*, *64*(1), 39–45. https://doi.org/10.1007/s00484-019-01791-1

Otani, H., Kaya, M., Tamaki, A., Watson, P., & Maughan, R. J. (2016). Effects of solar radiation on endurance exercise capacity in a hot environment. *European Journal of Applied Physiology*, *116*(4), 769–779. https://doi.org/10.1007/s00421-016-3335-9

Parabolix. (n.d.). *Fresnel Lens and Parabolic Reflectors*. Https://Www.Parabolixlight.Com/Fresnel-Lens-and-Parabolic-Reflectors.

Périard, J. D., Racinais, S., Sawka, M. N., & Périard, J. D. (2015). *Adaptations and mechanisms of human heat acclimation: Applications for competitive athletes and sports*. https://doi.org/10.1111/sms.12408

Périard, J. D., Travers, G. J. S., Racinais, S., & Sawka, M. N. (2016). Cardiovascular adaptations supporting human exercise-heat acclimation. *Autonomic Neuroscience*, *196*, 52–62. https://doi.org/10.1016/J.AUTNEU.2016.02.002

Pires António Filipe Vieira Dias. (2020). *ESTUDO DE MODELOS DE CONTROLO DE UMA CÂMARA CLIMÁTICA*.

Pryor, J. L., Pryor, R. R., Vandermark, L. W., Adams, E. L., VanScoy, R. M., Casa, D. J., Armstrong, L. E., Lee, E. C., DiStefano, L. J., Anderson, J. M., & Maresh, C. M. (2019). Intermittent exercise-heat exposures and intense physical activity sustain heat acclimation adaptations. *Journal of Science and Medicine in Sport*, *22*(1), 117–122. https://doi.org/10.1016/J.JSAMS.2018.06.009

Pryor, R. R., Pryor, J. L., Vandermark, L. W., Adams, E. L., Brodeur, R. M., Armstrong, L. E., Lee, E. C., Maresh, C. M., & Casa, D. J. (2021). Short term heat acclimation reduces heat strain during a first, but not second, consecutive exercise-heat exposure. *Journal of Science and Medicine in Sport*, *24*(8), 768–773. https://doi.org/10.1016/J.JSAMS.2021.03.020

Relf, R., Eichhorn, G., Waldock, K., Flint, M. S., Beale, L., & Maxwell, N. (2020). Validity of a wearable sweat rate monitor and routine sweat analysis techniques using heat acclimation. *Journal of Thermal Biology*, *90*, 102577. https://doi.org/10.1016/J.JTHERBIO.2020.102577

Sabahi, H., Tofigh, A. A., Kakhki, I. M., & Bungypoor-Fard, H. (2016). Design, construction and performance test of an efficient large-scale solar simulator for investigation of solar thermal collectors. *Sustainable Energy Technologies and Assessments*, *15*, 35–41. https://doi.org/10.1016/j.seta.2016.03.004

Salam, Z., Ramli, M. Z., & Zainal, T. (2014). A low cost solar array simulator using halogen tungsten bulb with temperature control capability. *2014 IEEE Conference on Energy Conversion (CENCON)*, 170–174. https://doi.org/10.1109/CENCON.2014.6967496

Samir, A., Mahgoub, A., Eliwa, A., Atia, D. M., El-Madany, H. T., El-Metwally, K., & Zahran, M. (2020). Design and Implementation of LED Solar Simulator. *WSEAS TRANSACTIONS ON POWER SYSTEMS*, *15*, 68–78. https://doi.org/10.37394/232016.2020.15.8

Sanwood. (n.d.). *SANWOOD Solar Simulator SM-4000*. Https://Www.Sanwood.Cc/Solar-Simulator-Pd6971043.Html.

Schleh, M. W., Ruby, B. C., & Dumke, C. L. (2018). Short term heat acclimation reduces heat stress, but is not augmented by dehydration. *Journal of Thermal Biology*, *78*, 227–234. https://doi.org/10.1016/J.JTHERBIO.2018.10.004

Singh, G., Virk, G., & Singla, A. (2016). *Modeling and Simulation of a Passive Lower-Body Mechanism for Rehabilitation*. https://www.researchgate.net/publication/283532449_Modeling_and_Simulation_of_a_Passive_Lower-Body_Mechanism_for_Rehabilitation

Sobek, S., & Werle, S. (2019). Comparative Review of Artificial Light Sources for Solar-Thermal Biomass Conversion Research Applications. *Ecological Chemistry and Engineering S*, *26*(3), 443–453. https://doi.org/10.1515/eces-2019-0033

Sun, C., Jin, Z., Song, Y., Chen, Y., Xiong, D., Lan, K., Huang, Y., & Zhang, M. (2022). LED-based solar simulator for terrestrial solar spectra and orientations. *Solar Energy*, *233*, 96–110. https://doi.org/10.1016/j.solener.2022.01.001

Tawfik, M., Tonnellier, X., & Sansom, C. (2018). Light source selection for a solar simulator for thermal applications: A review. *Renewable and Sustainable Energy Reviews*, *90*, 802–813. https://doi.org/10.1016/J.RSER.2018.03.059

Teo, W., Newton, M. J., & McGuigan, M. R. (2011). Circadian rhythms in exercise performance: Implications for hormonal and muscular adptation. *Journal of Sports Science and Medicine*.

TS-Space Systems. (n.d.). *Solar Simulator Basics - What Makes A Solar Simulator*. Solar Simulator Basics - What Makes A Solar Simulator. Retrieved August 11, 2022, from https://www.solar-simulator.info/what-is-solar-simulator.html

VELMURUGAN, P., & KALAIVANAN, R. (2016). Energy and exergy analysis in double-pass solar air heater. *Sadhana*. https://doi.org/10.1007/s12046-015-0456-5

Vitosevic, B. (2017). The circadian clock and human athletic performance. *The University Thought - Publication in Natural Sciences*, *7*(1), 1–7. https://doi.org/10.5937/univtho7-13650

Wang, J., Qiu, Y., Li, Q., Xu, M., & Wei, X. (2021). Design and experimental study of a 30 kWe adjustable solar simulator delivering high and uniform flux. *Applied Thermal Engineering*, *195*, 117215. https://doi.org/10.1016/j.applthermaleng.2021.117215

Wang, W. (2014a). *1_Simulate a sun for solar research*. https://www.diva-portal.org/smash/get/diva2:756274/FULLTEXT01.pdf

Wang, W. (2014b). *Simulate a "Sun" for solar research*. Toyal Institute of Technology .

Wang, W., Aichmayer, L., Garrido, J., & Laumert, B. (2017). Development of a Fresnel lens based high-flux solar simulator. *Solar Energy*, *144*, 436–444. https://doi.org/10.1016/j.solener.2017.01.050

Wat Electrical. (2018). *What is a Power Supply : Types for Electrical Circuits*. What Is a Power Supply : Types for Electrical Circuits. https://www.watelectrical.com/what-is-a-power-supply-and-types-of-power-supply-for-electrical-circuits/

Wikipedia. (n.d.). *Luminous efficacy*. Luminous Efficacy. Retrieved August 11, 2022, from https://en.wikipedia.org/wiki/Luminous_efficacy#cite_note-max-9

Xiao, J., Wei, X., Gilaber, R. N., Zhang, Y., & Li, Z. (2018). Design and characterization of a high-flux non-coaxial concentrating solar simulator. *Applied Thermal Engineering*, *145*, 201–211. https://doi.org/10.1016/j.applthermaleng.2018.09.050

Xiao, Y., Gao, Y., Wang, Y., & Meng, X. (2022). *Effects of solar radiation on thermal sensation and physical fatigue of the human body under heavy-load exercise*. https://doi.org/10.1177/1420326X20974736

Yamanaka, Y., Honma, K. I., Hashimoto, S., Takasu, N., Miyazaki, T., & Honma, S. (2006). Effects of physical exercise on human circadian rhythms. *Sleep and Biological Rhythms*, *4*(3), 199–206. https://doi.org/10.1111/j.1479-8425.2006.00234.x

Yandri, E. (2018). Uniformity characteristic and calibration of simple low cost compact halogen solar simulator for indoor experiments. *International Journal of Low-Carbon Technologies*, *13*(3), 218–230. https://doi.org/10.1093/ijlct/cty018

Yasmeen, S., & Liu, H. (2019). Evaluation of thermal comfort and heat stress indices in different countries and regions-A Review. *IOP Conference Series: Materials Science and Engineering*, *609*(5). https://doi.org/10.1088/1757-899X/609/5/052037

Zhang, S., & Zhu, N. (2021). Exercise heat acclimation causes human responses and safety performance improvements. *Journal of Thermal Biology*, *100*, 103042. https://doi.org/10.1016/J.JTHERBIO.2021.103042

Zhu, Q., Xuan, Y., Liu, X., Yang, L., Lian, W., & Zhang, J. (2020). A 130 kWe solar simulator with tunable ultra-high flux and characterization using direct multiple lamps mapping. *Applied Energy*, *270*, 115165. https://doi.org/10.1016/j.apenergy.2020.115165

# APPENDIX

## APPENDIX I

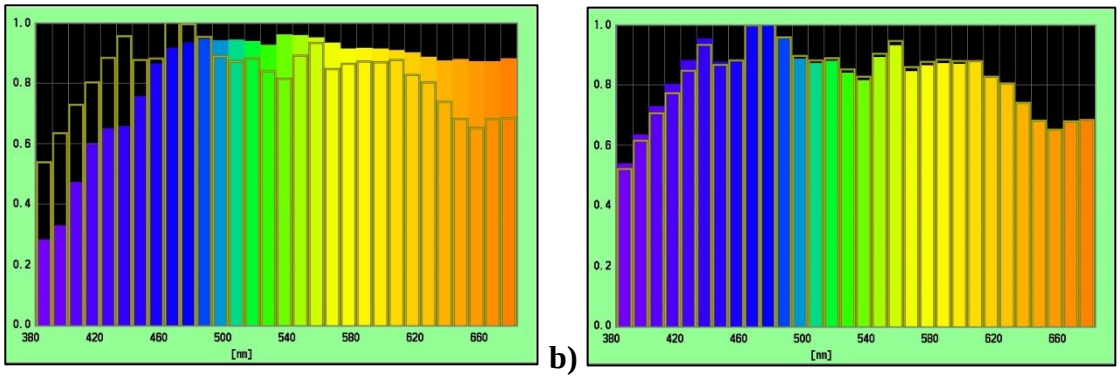


**a)** **b)**

**a)** Measured spectrums comparison, in a relative scale, of: the sun in a clear sky day; the studied luminaire, the closest to the light source measuring point $(X_1; Z_1)$.

**b)** Measured spectrums comparison, in a relative scale, of: the closest to the light source measuring point $(X_1; Z_1)$; the farthest to the light source measuring point $(X_6; Z_4)$.

## APPENDIX II

Measured values angle correction: **a)** calculations scheme **b)** comparsion between the readed values and the corrected values.

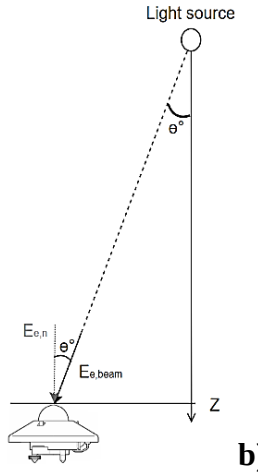


**a)** **b)**

| | | | X1 (0m) | X2 (0.1m) | X3 (0.2m) | X4 (0.3m) | X5 (0.4m) | X6 (0.5m) |
|---|---|---|---|---|---|---|---|---|
| z1 (0.55m) | Read | $E_v$ (lx) | 146000 | 108000 | 37800 | 13200 | 6880 | 4370 |
| | | $E_e$ (W/m$^2$) | 1160 | 1049 | 362 | 133 | 75 | 46 |
| | Corrected | $E_v$ (lx) | 146000 | 109771 | 40222 | 15036 | 8507 | 5906 |
| | | $E_e$ (W/m$^2$) | 1160 | 1066 | 385 | 151 | 93 | 62 |
| z2 (0.65m) | Read | $E_v$ (lx) | 105000 | 86300 | 35900 | 12000 | 7240 | 4410 |
| | | $E_e$ (W/m$^2$) | 1033 | 736 | 353 | 142 | 78 | 46 |
| | Corrected | $E_v$ (lx) | 105000 | 87315 | 37561 | 13216 | 8501 | 5564 |
| | | $E_e$ (W/m$^2$) | 1033 | 745 | 369 | 156 | 92 | 58 |
| z3 (0.75m) | Read | $E_v$ (lx) | 78800 | 70200 | 35400 | 14500 | 6880 | 4150 |
| | | $E_e$ (W/m$^2$) | 789 | 608 | 327 | 126 | 78 | 52 |
| | Corrected | $E_v$ (lx) | 78800 | 70821 | 36637 | 15617 | 7797 | 4988 |
| | | $E_e$ (W/m$^2$) | 789 | 613 | 338 | 136 | 88 | 62 |
| z4 (0.85m) | Read | $E_v$ (lx) | 61100 | 54000 | 33800 | 14300 | 7390 | 4490 |
| | | $E_e$ (W/m$^2$) | 583 | 516 | 312 | 160 | 78 | 53 |
| | Corrected | $E_v$ (lx) | 61100 | 54372 | 34723 | 15165 | 8167 | 5209 |
| | | $E_e$ (W/m$^2$) | 583 | 520 | 321 | 170 | 86 | 61 |

# APPENDIX III

Beam Angle calculations:

| | | $X_c$ (m) → $E_v$ (lx) | $X_c$ (m) → $E_e$ (W/m$^2$) | $E_v$ (lx) → $X_c$ (m) | $E_e$ (W/m$^2$) → $X_c$ (m) |
|---|---|---|---|---|---|
| z1 | X3 to X6: | y=120800.79*EXP(-6.32x) | y=1091.57*EXP(-5.96x) | x = - (ln(y/120800.79)/6.32) | x = - (ln(y/1091.57)/5.96) |
| | X1 to X3: | y=-1665981*(x^2) -195696*x+146000 | y=-29360*(x^2) +1998*x+1160 | x = (195696-RAÍZQ(195696^2 - 4*(-1665981)*(146000-y)))/(2*(- | x = (-1998-RAÍZQ(1998^2 - 4*(-29360)*(1160-y)))/(2*(-29360)) |
| z2 | X3 to X6: | y=107295.76*EXP(-6.17x) | y=1114.40*EXP(-6.09x) | x = - (ln(y/107295.76)/6.17) | x = - (ln(y/1114.40)/6.09) |
| | X1 to X3: | y=-1603484*(x^2) -16498*x+105000 | y=-4349*(x^2) -2448*x+1033 | x = (16498-RAÍZQ(16498^2 - 4*(-1603484)*(105000-y)))/(2*(- | x = (2448-RAÍZQ(2448^2 - 4*(-4349)*(1033-y)))/(2*(-4349)) |
| z3 | X3 to X6: | y=126398.36*EXP(-6.68x) | y=864.04*EXP(-5.50x) | x = - (ln(y/126398.36)/6.68) | x = - (ln(y/864.04)/5.50) |
| | X1 to X3: | y=-1310272*(x^2) + 51240*x+78800 | y=-4967*(x^2) -1260*x+789 | x = (-51240-RAÍZQ(51240^2 - 4*(-1310272)*(78800-y)))/(2*(- | x = (1260-RAÍZQ(1260^2 - 4*(-4967)*(789-y)))/(2*(-4967)) |
| z4 | (X3 to X6): | y=111345.90*EXP(-6.31x) | y=934.94*EXP(-5.63x) | x = - (ln(y/111345.90)/6.31) | x = - (ln(y/934.94)/5.63) |
| | (X1 to X3): | y=-646090*(x^2) -2667*x+61100 | y=-6780*(x^2) +44*x+583 | x = (2667-RAÍZQ(2667^2 - 4*(-646090)*(61100-y)))/(2*(-646090)) | x = (-44-RAÍZQ(44^2 - 4*(-6780)*(583-y)))/(2*(-6780)) |

| | | | | | Xc (m) | ɵ (°) | *Beam angle* (°) | *Beam angle* $_{average}$ (°) |
|---|---|---|---|---|---|---|---|---|
| z1 | $E_{v,max}$ (lx): | 146000 | $E_{v,max}$ / 2 (lx): | 73000 | 0.159 | 16.09 | 32.19 | 29.69 |
| | $E_{e,max}$ (W/m$^2$): | 1160 | $E_{e,max}$/ 2 (W/m$^2$): | 580 | 0.179 | 17.99 | 35.99 | |
| z2 | $E_{v,max}$ (lx): | 105000 | $E_{v,max}$ / 2 (lx): | 52500 | 0.176 | 15.14 | 30.28 | |
| | $E_{e,max}$ (W/m$^2$): | 1033 | $E_{e,max}$/ 2 (W/m$^2$): | 516.5 | 0.163 | 14.12 | 28.24 | |
| z3 | $E_{v,max}$ (lx): | 78800 | $E_{v,max}$ / 2 (lx): | 39400 | 0.194 | 14.51 | 29.01 | |
| | $E_{e,max}$ (W/m$^2$): | 789 | $E_{e,max}$/ 2 (W/m$^2$): | 394.5 | 0.182 | 13.66 | 27.31 | |
| z4 | $E_{v,max}$ (lx): | 61100 | $E_{v,max}$ / 2 (lx): | 30550 | 0.205 | 13.56 | 27.11 | |
| | $E_{e,max}$ (W/m$^2$): | 583 | $E_{e,max}$/ 2 (W/m$^2$): | 291.5 | 0.207 | 13.69 | 27.37 | |

# APPENDIX IV

Conversion to polar coordinates and *LDT Editor* input data calculations:

| $ɵ_i$ (°) | $z_j$ (m) | $d_{ij}$ (m) | $E_{e,ij}$ (W/m2) | $E_{v,ij}$ (lx) | $I_{v,ij}$ (cd) | $I_{v,average}$ (cd) | $I_{v,average}$ (cd/klm$_{lamp}$) |
|---|---|---|---|---|---|---|---|
| 0 | 0.55 | 0.55 | 1160.0 | 146000.0 | 44165.0 | 44249.31 | 903.0471939 |
| | 0.65 | 0.65 | 1033.0 | 105000.0 | 44362.5 | | |
| | 0.75 | 0.75 | 789.0 | 78800.0 | 44325.0 | | |
| | 0.85 | 0.85 | 583.0 | 61100.0 | 44144.8 | | |
| 3 | 0.55 | 0.5508 | 1193.2 | 138975.0 | 42155.4 | 43326.34 | 884.2109918 |
| | 0.65 | 0.6509 | 944.6 | 102577.3 | 43457.9 | | |
| | 0.75 | 0.7510 | 729.8 | 78789.7 | 44440.9 | | |
| | 0.85 | 0.8512 | 570.1 | 59699.1 | 43251.1 | | |
| 6 | 0.55 | 0.55303 | 1177.4 | 129120.1 | 39490.3 | 40959.35 | 835.9051013 |
| | 0.65 | 0.65358 | 845.5 | 96388.9 | 41174.2 | | |
| | 0.75 | 0.754131 | 654.7 | 74697.3 | 42481.4 | | |
| | 0.85 | 0.854682 | 529.7 | 55705.0 | 40691.5 | | |
| 9 | 0.55 | 0.5569 | 1111.3 | 116310.5 | 36066.5 | 37011.28 | 755.3323462 |
| | 0.65 | 0.6581 | 734.9 | 86306.7 | 37379.3 | | |
| | 0.75 | 0.7593 | 562.8 | 66397.9 | 38285.7 | | |
| | 0.85 | 0.8606 | 460.9 | 49031.0 | 36313.5 | | |
| 12 | 0.55 | 0.562287 | 992.3 | 100352.9 | 31728.3 | 31243.62 | 637.6249417 |
| | 0.65 | 0.664521 | 611.8 | 72112.2 | 31843.9 | | |
| | 0.75 | 0.766755 | 453.1 | 53669.4 | 31553.0 | | |
| | 0.85 | 0.86899 | 362.1 | 39528.0 | 29849.3 | | |
| 15 | 0.55 | 0.5694 | 816.8 | 80977.2 | 26254.3 | 22716.78 | 463.6077014 |
| | 0.65 | 0.6729 | 474.7 | 53486.3 | 24220.4 | | |
| | 0.75 | 0.7765 | 286.1 | 33016.7 | 19905.3 | | |
| | 0.85 | 0.8800 | 259.4 | 26456.3 | 20487.1 | | |
| 18 | 0.55 | 0.578304 | 579.4 | 57823.6 | 19338.3 | 15989.48 | 326.3158526 |
| | 0.65 | 0.68345 | 307.9 | 29151.3 | 13616.7 | | |
| | 0.75 | 0.788597 | 226.2 | 24818.5 | 15434.3 | | |
| | 0.85 | 0.893743 | 197.5 | 19490.6 | 15568.7 | | |
| 21 | 0.55 | 0.5891 | 310.2 | 31811.6 | 11041.0 | 11474.16 | 234.1666293 |
| | 0.65 | 0.6962 | 243.8 | 23014.0 | 11156.2 | | |
| | 0.75 | 0.8034 | 177.4 | 18472.4 | 11921.8 | | |
| | 0.85 | 0.9105 | 148.9 | 14207.7 | 11777.7 | | |
| 24 | 0.55 | 0.60205 | 253.6 | 25700.9 | 9315.7 | 9107.607 | 185.8695355 |
| | 0.65 | 0.711514 | 191.3 | 17993.3 | 9109.1 | | |
| | 0.75 | 0.820977 | 137.7 | 13583.3 | 9155.2 | | |
| | 0.85 | 0.930441 | 111.0 | 10223.2 | 8850.4 | | |
| 27 | 0.55 | 0.6173 | 205.4 | 20553.5 | 7831.6 | 7198.686 | 146.9119656 |
| | 0.65 | 0.7295 | 148.3 | 13903.5 | 7399.2 | | |
| | 0.75 | 0.8417 | 105.6 | 9842.6 | 6973.8 | | |
| | 0.85 | 0.9540 | 81.6 | 7241.3 | 6590.1 | | |
| 30 | 0.55 | 0.635085 | 164.5 | 16236.7 | 6548.8 | 5654.887 | 115.4058496 |
| | 0.65 | 0.750555 | 113.4 | 10592.3 | 5967.0 | | |
| | 0.75 | 0.866025 | 79.8 | 7007.0 | 5255.3 | | |
| | 0.85 | 0.981495 | 59.0 | 5033.0 | 4848.5 | | |

| $ɵ_i$ (°) | $z_j$ (m) | $d_{ij}$ (m) | $E_{e,ij}$ (W/m2) | $E_{v,ij}$ (lx) | $I_{v,ij}$ (cd) | $I_{v,average}$ (cd) | $I_{v,average}$ (cd/klm$_{lamp}$) |
|---|---|---|---|---|---|---|---|
| 33 | 0.55 | 0.6558 | 129.9 | 12639.2 | 5435.8 | 4404.951 | 89.89696321 |
| | 0.65 | 0.7750 | 85.2 | 7933.9 | 4765.7 | | |
| | 0.75 | 0.8943 | 59.3 | 4883.7 | 3905.6 | | |
| | 0.85 | 1.0135 | 41.8 | 3419.7 | 3512.7 | | |
| 36 | 0.55 | 0.679837 | 100.9 | 9666.6 | 4467.7 | 3393.571 | 69.25654839 |
| | 0.65 | 0.803444 | 62.8 | 5822.9 | 3758.8 | | |
| | 0.75 | 0.927051 | 43.1 | 3318.3 | 2851.8 | | |
| | 0.85 | 1.050658 | 28.9 | 2261.1 | 2495.9 | | |
| 39 | 0.55 | 0.7077 | 76.8 | 7237.9 | 3625.2 | 2577.478 | 52.60159015 |
| | 0.65 | 0.8364 | 45.2 | 4170.1 | 2917.2 | | |
| | 0.75 | 0.9651 | 30.6 | 2186.8 | 2036.7 | | |
| | 0.85 | 1.0937 | 19.4 | 1446.8 | 1730.8 | | |
| 42 | 0.55 | 0.740098 | 57.0 | 5282.2 | 2893.3 | 1922.534 | 39.23538801 |
| | 0.65 | 0.874661 | 31.6 | 2899.4 | 2218.2 | | |
| | 0.75 | 1.009225 | 21.1 | 1388.8 | 1414.5 | | |
| | 0.85 | 1.143788 | 12.6 | 889.9 | 1164.2 | | |
| 45 | 0.55 | 0.7778 | 41.2 | 3736.5 | 2260.6 | 1401.527 | 28.60259042 |
| | 0.65 | 0.9192 | 21.3 | 1944.7 | 1643.2 | | |
| | 0.75 | 1.0607 | 14.0 | 843.2 | 948.6 | | |
| | 0.85 | 1.2021 | 7.8 | 521.6 | 753.7 | | |
| 48 | 0.55 | 0.821962 | 28.6 | 2543.8 | 1718.6 | 992.4749 | 20.25459024 |
| | 0.65 | 0.97141 | 13.7 | 1247.9 | 1177.6 | | |
| | 0.75 | 1.120857 | 8.8 | 484.5 | 608.6 | | |
| | 0.85 | 1.270305 | 4.6 | 288.2 | 465.0 | | |
| 51 | 0.55 | 0.8740 | 19.1 | 1651.4 | 1261.4 | 677.2975 | 13.822397 |
| | 0.65 | 1.0329 | 8.4 | 758.1 | 808.7 | | |
| | 0.75 | 1.1918 | 5.3 | 259.9 | 369.2 | | |
| | 0.85 | 1.3507 | 2.5 | 148.0 | 269.9 | | |
| 54 | 0.55 | 0.935716 | 12.0 | 1009.9 | 884.2 | 440.7551 | 8.995002507 |
| | 0.65 | 1.105846 | 4.8 | 429.8 | 525.6 | | |
| | 0.75 | 1.275976 | 3.0 | 127.9 | 208.3 | | |
| | 0.85 | 1.446106 | 1.3 | 69.3 | 144.9 | | |
| 57 | 0.55 | 1.0098 | 7.0 | 572.1 | 583.4 | 269.5973 | 5.501984702 |
| | 0.65 | 1.1935 | 2.5 | 223.1 | 317.8 | | |
| | 0.75 | 1.3771 | 1.5 | 56.4 | 107.0 | | |
| | 0.85 | 1.5607 | 0.6 | 28.8 | 70.2 | | |
| 60 | 0.55 | 1.1 | 3.7 | 293.3 | 354.9 | 151.8886 | 3.09976652 |
| | 0.65 | 1.3 | 1.2 | 103.2 | 174.5 | | |
| | 0.75 | 1.5 | 0.7 | 21.5 | 48.5 | | |
| | 0.85 | 1.7 | 0.2 | 10.3 | 29.7 | | |
| 63 | 0.55 | 1.2115 | 1.8 | 131.6 | 193.2 | 76.52133 | 1.56165979 |
| | 0.65 | 1.4317 | 0.5 | 40.9 | 83.9 | | |
| | 0.75 | 1.6520 | 0.3 | 6.8 | 18.5 | | |
| | 0.85 | 1.8723 | 0.1 | 3.0 | 10.5 | | |

| $\theta_i$ (°) | $z_j$ (m) | $d_{ij}$ (m) | $E_{e,ij}$ (W/m2) | $E_{v,ij}$ (lx) | $I_{v,ij}$ (cd) | $I_{v,average}$ (cd) | $I_{v,average}$ (cd/klm$_{lamp}$) |
|---|---|---|---|---|---|---|---|
| 66 | 0.55 | 1.352226 | 0.7 | 49.1 | 89.9 | 32.95921 | 0.672636979 |
| | 0.65 | 1.598086 | 0.2 | 13.1 | 33.6 | | |
| | 0.75 | 1.843945 | 0.1 | 1.6 | 5.6 | | |
| | 0.85 | 2.089804 | 0.0 | 0.7 | 2.9 | | |
| 69 | 0.55 | 1.5347 | 0.2 | 14.1 | 33.2 | 11.29783 | 0.230568006 |
| | 0.65 | 1.8138 | 0.0 | 3.1 | 10.2 | | |
| | 0.75 | 2.0928 | 0.0 | 0.3 | 1.2 | | |
| | 0.85 | 2.3719 | 0.0 | 0.1 | 0.5 | | |
| 72 | 0.55 | 1.779837 | 0.0 | 2.7 | 8.6 | 2.730269 | 0.055719765 |
| | 0.65 | 2.103444 | 0.0 | 0.5 | 2.1 | | |
| | 0.75 | 2.427051 | 0.0 | 0.0 | 0.1 | | |
| | 0.85 | 2.750658 | 0.0 | 0.0 | 0.1 | | |
| 75 | 0.55 | 2.1250 | 0.0 | 0.3 | 1.3 | 0.372908 | 0.007610358 |
| | 0.65 | 2.5114 | 0.0 | 0.0 | 0.2 | | |
| | 0.75 | 2.8978 | 0.0 | 0.0 | 0.0 | | |
| | 0.85 | 3.2841 | 0.0 | 0.0 | 0.0 | | |
| 78 | 0.55 | 2.645354 | 0.0 | 0.0 | 0.1 | 0.01841 | 0.000375709 |
| | 0.65 | 3.126327 | 0.0 | 0.0 | 0.0 | | |
| | 0.75 | 3.607301 | 0.0 | 0.0 | 0.0 | | |
| | 0.85 | 4.088274 | 0.0 | 0.0 | 0.0 | | |
| 81 | 0.55 | 3.5158 | 0.0 | 0.0 | 0.0 | 0.000115 | 2.33724E-06 |
| | 0.65 | 4.1551 | 0.0 | 0.0 | 0.0 | | |
| | 0.75 | 4.7943 | 0.0 | 0.0 | 0.0 | | |
| | 0.85 | 5.4336 | 0.0 | 0.0 | 0.0 | | |
| 84 | 0.55 | 5.261725 | 0.0 | 0.0 | 0.0 | 3.65E-09 | 7.45476E-11 |
| | 0.65 | 6.218402 | 0.0 | 0.0 | 0.0 | | |
| | 0.75 | 7.175079 | 0.0 | 0.0 | 0.0 | | |
| | 0.85 | 8.131756 | 0.0 | 0.0 | 0.0 | | |
| 87 | 0.55 | 10.5090 | 0.0 | 0.0 | 0.0 | 5.23E-23 | 1.06642E-24 |
| | 0.65 | 12.4198 | 0.0 | 0.0 | 0.0 | | |
| | 0.75 | 14.3305 | 0.0 | 0.0 | 0.0 | | |
| | 0.85 | 16.2412 | 0.0 | 0.0 | 0.0 | | |

# APPENDIX V

*LDT Editor interface*:

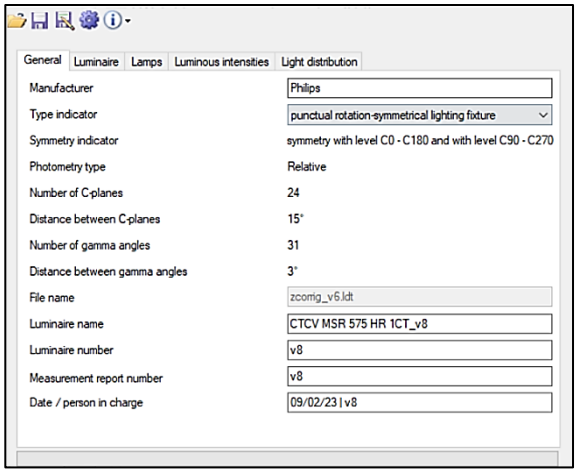


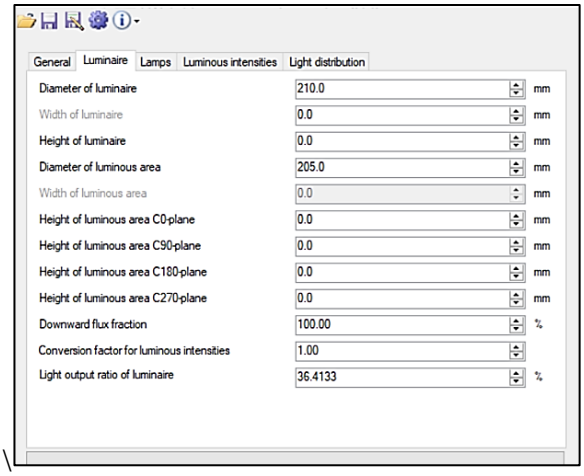


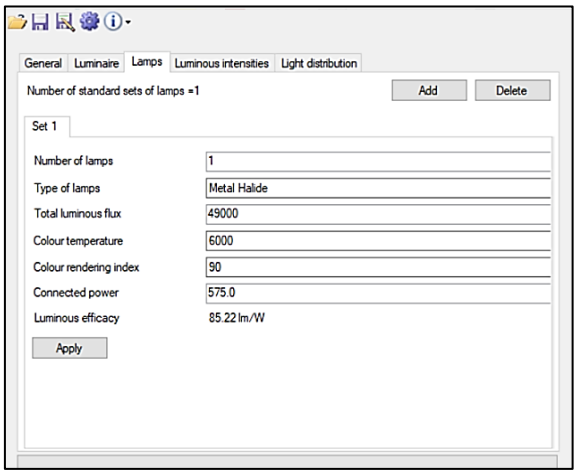

General | Luminaire | Lamps | Luminous intensities | Light distribution

| | C0° | C15° | C30° | C45° | C60° | C75° | C90° |
|---|---|---|---|---|---|---|---|
| G0° | 903.05 | 903.05 | 903.05 | 903.05 | 903.05 | 903.05 | 903.05 |
| G3° | 884.21 | 884.21 | 884.21 | 884.21 | 884.21 | 884.21 | 884.21 |
| G6° | 835.91 | 835.91 | 835.91 | 835.91 | 835.91 | 835.91 | 835.91 |
| G9° | 755.33 | 755.33 | 755.33 | 755.33 | 755.33 | 755.33 | 755.33 |
| G12° | 637.62 | 637.62 | 637.62 | 637.62 | 637.62 | 637.62 | 637.62 |
| G15° | 463.61 | 463.61 | 463.61 | 463.61 | 463.61 | 463.61 | 463.61 |
| G18° | 326.31 | 326.31 | 326.31 | 326.31 | 326.31 | 326.31 | 326.31 |
| G21° | 234.17 | 234.17 | 234.17 | 234.17 | 234.17 | 234.17 | 234.17 |
| G24° | 185.87 | 185.87 | 185.87 | 185.87 | 185.87 | 185.87 | 185.87 |
| G27° | 146.91 | 146.91 | 146.91 | 146.91 | 146.91 | 146.91 | 146.91 |
| G30° | 115.41 | 115.41 | 115.41 | 115.41 | 115.41 | 115.41 | 115.41 |
| G33° | 89.9 | 89.9 | 89.9 | 89.9 | 89.9 | 89.9 | 89.9 |
| G36° | 69.27 | 69.27 | 69.27 | 69.27 | 69.27 | 69.27 | 69.27 |
| G39° | 52.6 | 52.6 | 52.6 | 52.6 | 52.6 | 52.6 | 52.6 |
| G42° | 39.24 | 39.24 | 39.24 | 39.24 | 39.24 | 39.24 | 39.24 |
| G45° | 28.6 | 28.6 | 28.6 | 28.6 | 28.6 | 28.6 | 28.6 |
| G48° | 20.26 | 20.26 | 20.26 | 20.26 | 20.26 | 20.26 | 20.26 |
| G51° | 13.82 | 13.82 | 13.82 | 13.82 | 13.82 | 13.82 | 13.82 |
| G54° | 9 | 9 | 9 | 9 | 9 | 9 | 9 |
| G57° | 5.5 | 5.5 | 5.5 | 5.5 | 5.5 | 5.5 | 5.5 |
| G60° | 3.1 | 3.1 | 3.1 | 3.1 | 3.1 | 3.1 | 3.1 |
| G63° | 1.56 | 1.56 | 1.56 | 1.56 | 1.56 | 1.56 | 1.56 |
| G66° | 0.67 | 0.67 | 0.67 | 0.67 | 0.67 | 0.67 | 0.67 |
| G69° | 0.23 | 0.23 | 0.23 | 0.23 | 0.23 | 0.23 | 0.23 |
| G72° | 0.06 | 0.06 | 0.06 | 0.06 | 0.06 | 0.06 | 0.06 |
| G75° | 0.01 | 0.01 | 0.01 | 0.01 | 0.01 | 0.01 | 0.01 |
| G78° | 0 | 0 | 0 | 0 | 0 | 0 | 0 |
| G81° | 0 | 0 | 0 | 0 | 0 | 0 | 0 |
| G84° | 0 | 0 | 0 | 0 | 0 | 0 | 0 |
| G87° | 0 | 0 | 0 | 0 | 0 | 0 | 0 |
| G90° | 0 | 0 | 0 | 0 | 0 | 0 | 0 |

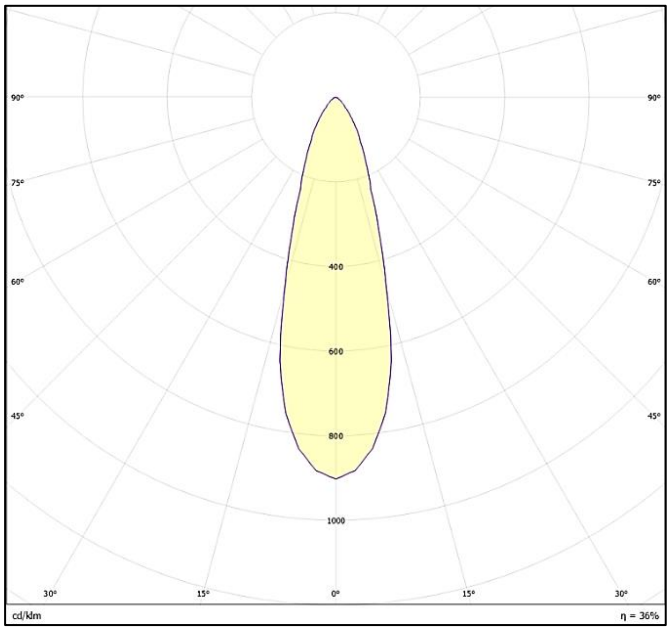


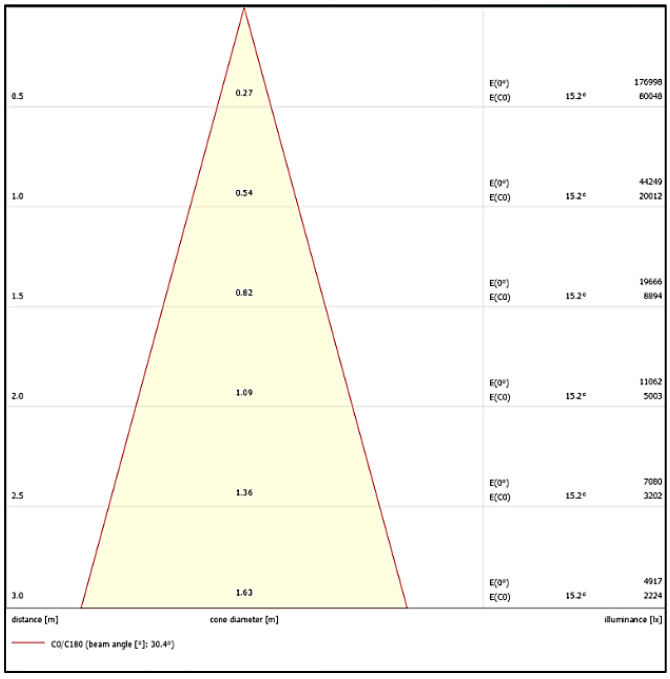

## APPENDIX VI

Lamp's configuration in *DIALux:*

| | |
|---|---|
| P | 575.0 W |
| $\Phi_{Lâmpada}$ | 49000 lm |
| $\Phi_{Luminária}$ | 17843 lm |
| η | 36.41 % |
| Rendimento luminoso | 31.0 lm/W |
| CCT | 6000 K |
| CRI | 90 |


## APPENDIX VII

Model validation – simulated values in the four Z planes: **a)** Z1; **b)** Z2; **c)** Z3; **d)** Z4.

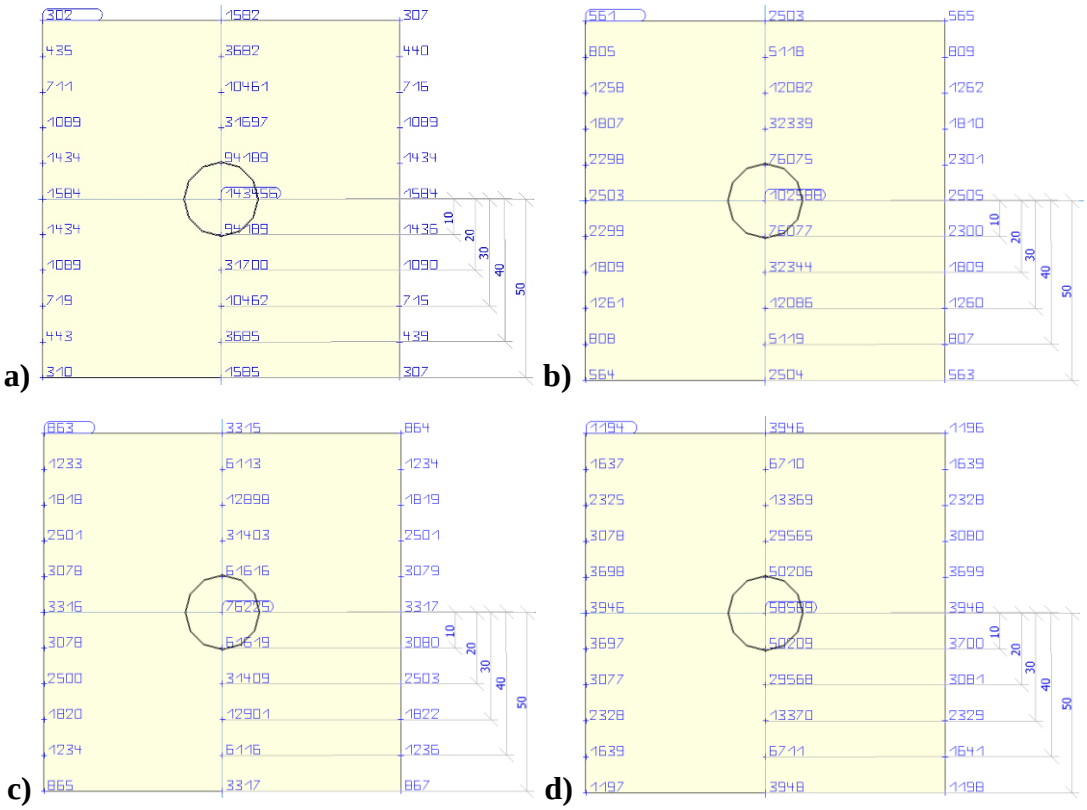

## APPENDIX VIII

Scheme of the climate chamber's architecture plan:

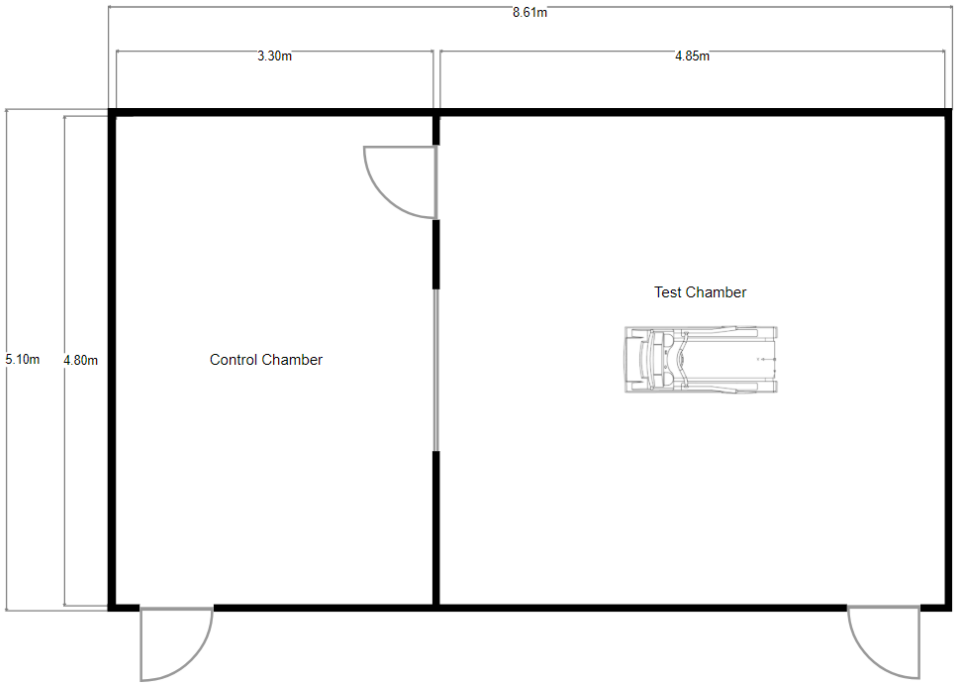


## APPENDIX IX

Solar Simulator's configurations in *DIALux*: **a)** Configuration A; **b)** Configuration B; **c)** Configuration C; **d)** Configuration D; **e)** Configuration E.

**a)** 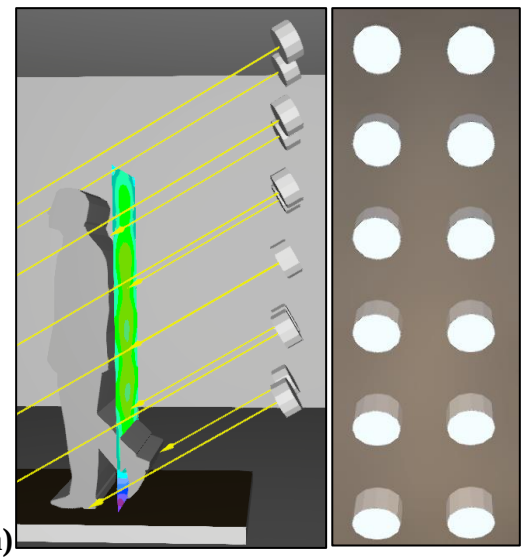

**b)** 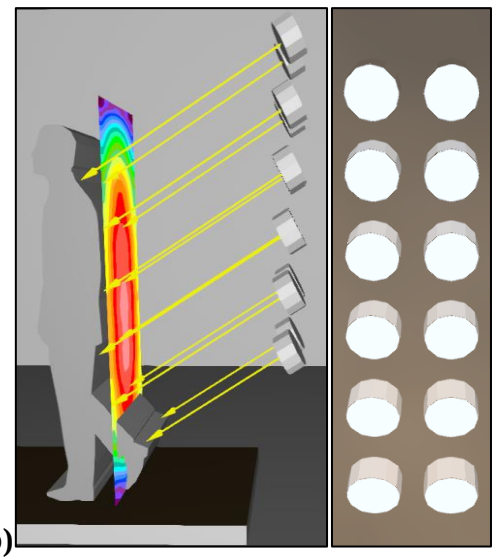

c) 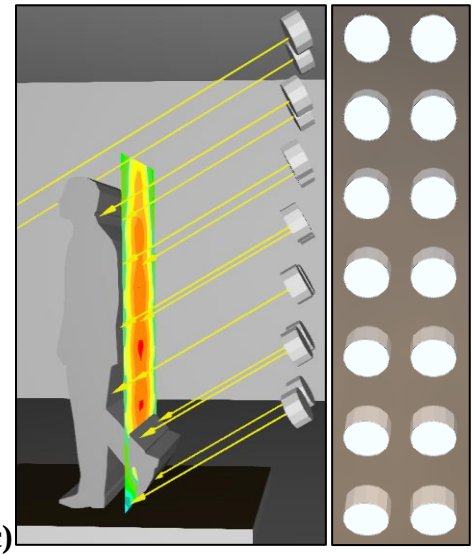

d) 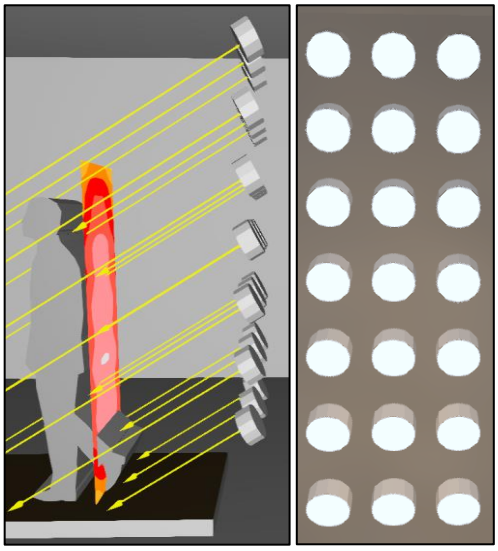

e)